

# Small Carbon Particle Generator

San Diego State University  
COLLEGE OF ENGINEERING  
Department of Mechanical Engineering

*ME490B-Senior Design Project*

Instructor: Dr. Moon  
Advisers: Dr. Fletcher Miller and Dr. Arlon Hunt  
Sponsor: Google.org

May 22, 2009

Daniel Cassinis  
Chris Renner

## **Table of Contents**

|   |              |
|---|--------------|
| <b>Abstract</b>   | <b>2</b>     |
| <b>Introduction/Background</b>                                | <b>2-4</b>   |
| <b>Literature Review</b>                                      | <b>4</b>     |
| <b>Methodology</b>  | <b>4-12</b>  |
| <b>ME 490B Final Design</b>                                   | <b>12-23</b> |
| <b>Results</b>  | <b>24-30</b> |
| <b>Conclusion</b>   | <b>31</b>    |
| <b>Acknowledgements</b>                                       | <b>32</b>    |
| <b>References</b>   | <b>33</b>    |
| <b>Appendix 1</b>   |              |
| <b>Derivation of Fourier's Law in Cylindrical Coordinates</b> | <b>34-37</b> |
| <b>Table 1. Insulation Thickness and Temperatures</b>         | <b>38</b>    |
| <b>Permeability Data</b>                                      | <b>39-40</b> |
| <b>Two-Dimensional Conduction Code</b>                        | <b>41-47</b> |
| <b>Table 2. Nozzle Data</b>                                   | <b>48</b>    |

## Abstract

The need for more efficient ways to produce energy is a major focus in the 21st century. Through the use of carbon particles, solar flux, and a Brayton cycle; energy can be produced with greater efficiency compared to existing solar thermal or photovoltaic efficiency. This project focuses on the design and creation of a small carbon particle generator. Pyrolysis of methane and extraction of carbon particles will be implemented through the use of a wall less reactor. Inert gas, nitrogen, flows into the outer chamber to be defused through blanketed insulation, heating coils and a porous ceramic to react with the methane flowing through the middle of the ceramic tubing. Not much research has been done in this area before other than original tests. Final assembly is nearing completion and all components have been bench tested. Trial pyrolysis runs will be conducted in the following week.

## Background/Introduction

This project is the first half of a two year venture that is tasked with creating a wall-less small carbon particle generator. The first year of the project involves the creation of a working prototype. Starting with methane gas ( $CH_4$ ), heat is added to break the hydrogen and carbon bonds. This reaction is referred to as pyrolysis, defined as the “decomposition or transformation of a compound caused by heat” [1]. The simplified chemical equation is given as



The small carbon particles will be suspended in air forming a particle suspension. Research conducted in the late 1970's by Dr. Hunt at Lawrence Berkeley Laboratory found that “a dispersion of small absorbing particles forms an ideal system to collect radiant energy, transform it to heat, and efficiently transfer the heat to a surrounding fluid” [2]. In other words, when subjected to solar flux a small carbon particle suspension can efficiently transfer energy to heat the suspension fluid.

The relevance of this design problem becomes clear when it is applied to the thermal solar power generation industry. According to the Energy Information Administration's data from the year 2006, the United States generated 1,990,926 thousand megawatt hours of power from coal, a non-renewable resource. In the same year 96,423 thousand megawatt hours of power was generated with renewable resources including solar and wind. When compared to the total power generated for 2006, coal power accounted for 49.0 % while renewable resources accounted for 2.37% [3]!

Today's society feels the full effect of the dependence on a limited fuel source with the rise in gas and electric prices. The need for cheap, efficient sources of energy is clear. However, these cheap fuel sources must also be clean and environment friendly. Current scientific evidence indicates that global warming is indeed a real phenomena occurring in our lifetime. This is where the relevance of our design lies. The energy from sunlight hitting the Earth's surface is

approximately  $1 \text{ kw}/ \text{m}^2$  [4]. It is in the solar power generation industry where this abundant energy source is captured and converted to usable electricity.

Currently, liquids such as water or molten salt are used to capture solar flux in solar thermal power cycles. Mirrors direct the solar flux to a system that heats the liquid, pumps it through a turbine creating electricity. The efficiency from such systems is roughly 15% [5]. The small particle generator our team is designing will be used in an open air Brayton power cycle in which air is the working fluid. Figure 1 shows the configuration of this power cycle. Early prototypes for several system components and theoretical analysis of this cycle performed in the late 1970's by Dr. Hunt demonstrated an efficiency of 36%. Depending on the scale of power generation and assumptions made, this value could vary by approximately 10% [2]. The potential for obtaining efficiencies on this scale in the solar power industry compared to current technology is the reason this project is important.

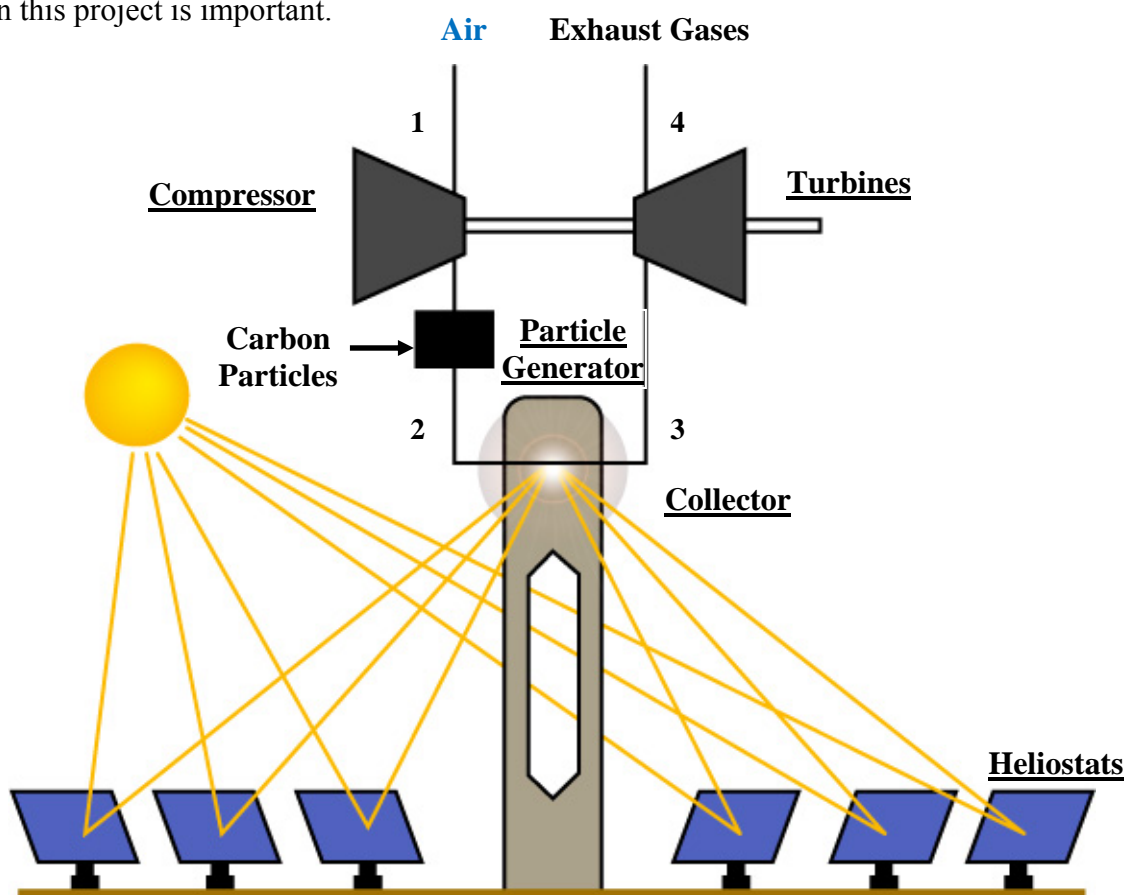


Fig. 1. Open Brayton cycle solar thermal power plant.

An early prototype of a small carbon particle generator was created in the 1980's by advisors Dr. Miller and Dr. Hunt. Argon gas was pyrolyzed by passing it through a quartz tube inside of a tube furnace at a temperature of approximately  $1000 \text{ }^\circ\text{C}$ . The design was simple and functional but proved messy, requiring constant cleaning to remove carbon build up since the reaction occurred at the highest temperature region of the device, the walls.

Our goals for this project were to use methane, nitrogen, and air to end up with a particle suspension. Our design has the ability to control the pressure and flow rates of the gases as well as the temperature of the reactor so that particle size may be manipulated. Particle reaction is to occur in the center of the device away from the walls to allow for clean operation.

### **Literature Review**

Several sources on the topic of small particle generators were used. The only information on the topic was from the previous experiment back in late 1970's. The article used was one of our advisor's. The article, "Small Particle Heat Exchangers" and the report "Phase I Report" by Arlon J.Hunt, helped tremendously and gave detailed background into the project. Both helped define expectations of the outcome and also the implementation of the particle generator in a solar flux power plant.

Two more articles were used that were written by Dr. Hunt on the same topic of "Small Particle Generation". Both articles had similar information about the creation of carbon particles. Just like the first article discussed both deal with the use of the carbon in a solar flux power plant. This helped the group immensely and gave a template on how to implement our design.

However helpful these three articles were, there was not any information on the pyrolysis of methane specifically in the articles. This is one of the main differences from the original experiment conducted in the 1970's. The book, "Pyrolysis: Theory and Industrial Practice" by Lyle F. Albright, helped tremendously in the design of our particle generator. The article helped narrow down how long it takes the reaction to occur. The book gives a general range of 1.0 seconds to 0.1 seconds for the reaction to occur. The reaction temperature of 900 degrees Celsius was also discerned from this book [6]. The effects that gravity has on the gas itself also affect our design inlets of the gas. The use of a wall-less reactor was discussed in the book as well which helped validate our initial design idea.

Another Text used was instrumental in the design of the inner ceramic tube. From, "Transport Phenomena" by Bird, analysis of flow through a porous ceramic was discussed. Examples helped in determining wall thickness and pressure drops. This was key to understanding flow in the chamber.

### **Initial Design Methodology**

Our initial design began with no existing information on small particle generators using methane other than the temperature necessary for pyrolysis, 900 to 1000°C. The objectives of the design were to use methane and nitrogen or argon gases to end up with a particle suspension. The pressure and flow rates of the gases needed to be controllable. The reaction chamber temperature needed to be controllable. Most importantly, reaction must take place away from the reactor walls meaning that the highest temperature must occur towards the center of the device.

The system was broken down into three subsystems; gas control, reaction chamber, and heating. The gases used are nitrogen and methane. Once the device is functioning, air may be added into the chamber as suggested by Dr. Hunt. All gases are commercially available and their pressures

easily controlled by use of pressure regulators. The mass flow rates of gases are controlled using digital gas flow controllers connected inline between the regulated gas supply and the reaction chamber. Dr. Miller is currently in possession of two controllers that will be used in our design. Figure 2 provides an overview of the reaction chamber system.

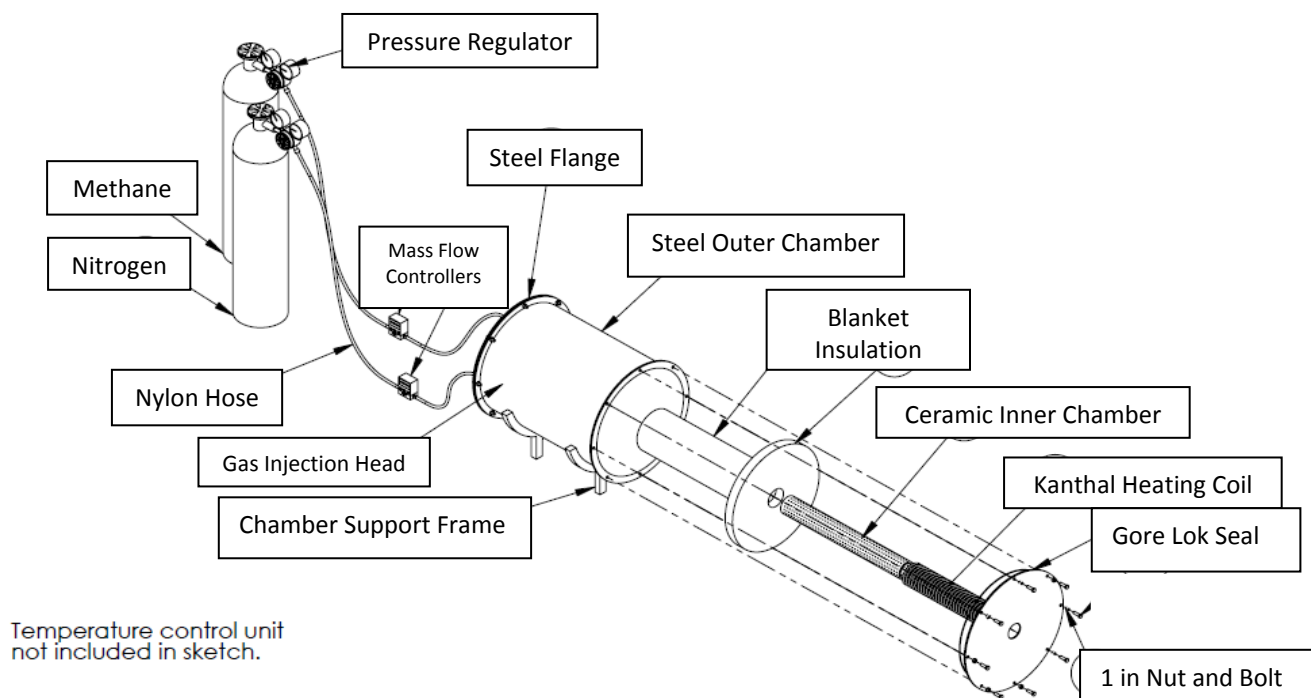


Fig. 2. Wall-less small particle generator design overview.

The next subsystem is the reaction chamber itself. Factors to consider in the design of the reaction chamber are geometry, how the gases are mixed, and how the gases are going to be heated. First, different geometries for the reaction chamber were considered including a square cross-section, a spherical shape, and cylindrical cross-section. We decided to pursue a cylindrical cross-section for the reaction chamber due to the availability of cylindrical piping elements as well as readily available equations for stress calculations when assuming the chamber is a thin walled pressure vessel with sealed ends. Another consideration is that with a cylindrical reaction chamber gas flow is easier to visualize and turbulent flow regions due to sharp corners or bends are minimized with this geometry (areas of highest probability for carbon coke buildup). The gas flow dynamics in the chamber could be further explored by future engineering teams using advanced thermofluids principles and computational fluid dynamic software packages to fully model and understand the gas behaviors and energy flow in the system. This is currently being performed by one of Dr. Miller's graduate students.

The most important design objective as recognized by our team is keeping the reacting gases away from the walls of the inner chamber. How the gases mix was considered next. We looked at injecting both gases into the chamber and how they might react given the location and method of heating. If the gases were to be heated in the center of the chamber using heating coils, the pyrolysis reaction would occur on the surface of the high temperature coils. Over time carbon buildup would force periodic disassembly and cleaning of the chamber. Since the device is to operate at steady state with minimal cleaning or maintenance an arrangement of mixing the two gases randomly with direct heating was ruled out.

What was needed for the design was to keep the gases separate in the reaction chamber and mix them in a controlled manner. It was from this goal that we began to pursue an inner and outer reaction chamber design. An inner cylinder would reside within an outer cylinder, with one gas flowing into the inner chamber and the other flowing into the outer chamber. From this point, the gases would be allowed to mix by passing through slits or injectors from one tube to the other. If the nitrogen were to be heated to the necessary temperature for reaction, it could be injected into the chamber containing the methane and the pyrolysis reaction would occur. With this idea in mind, we evaluated passing the gas from one chamber to the other through slits or small injectors. This presented the problem of predicting how the gases would flow near the wall. The possibility of turbulence causing the reaction to occur in direct contact with the wall in a localized area was a high probability scenario that would force disassembly and cleaning.

Ideally, for the reaction to take place away from the walls, a gas passing from one chamber to the other through the inner tube would have to occur at every point along the inner tube's surface. This would create a boundary layer of gas that would prevent the reaction from reaching the walls. It was at this point that material selection was researched. The most promising of materials for the inner chamber was a porous ceramic. With a pressure gradient across the thickness of the tube, a gas can be diffused through the small pores. If gas flow rates and pressures are correct, a gas passing from the outer chamber can be diffused into the inner chamber. If this gas is at high temperature, the reaction can be carried out in the inner chamber away from the heating source and would remain off of the walls because of the protective boundary layer due to the constant inflow of gas.

The difficulty with this design is determining the correct gas flow rates and pressures to achieve usable results. At this point in the design, our team began researching gas diffusion through a porous ceramic, ideally a cylindrical porous ceramic tube. After finding little to no information on the subject, our advisor found a near identical system in "Transport Phenomena." Equation (2) gives the volumetric flow rate through a porous ceramic

$$Q = \frac{\pi k h (P_2^2 - P_1^2)}{\mu P_1 \ln(r_2 / r_1)} + Q_i \quad (2)$$

where  $Q$  is the total volumetric flow rate,  $K$  is the permeability of the porous medium,  $\mu$  is the viscosity of the fluid,  $P$  is the pressure ( $P_2$  outside the tube,  $P_1$  inside),  $r$  is the radius ( $r_2$  outside radius,  $r_1$  inside radius), and  $Q_i$  is the initial flow rate entering the ceramic tube [8]. The configuration of this system is shown in Fig. 3.

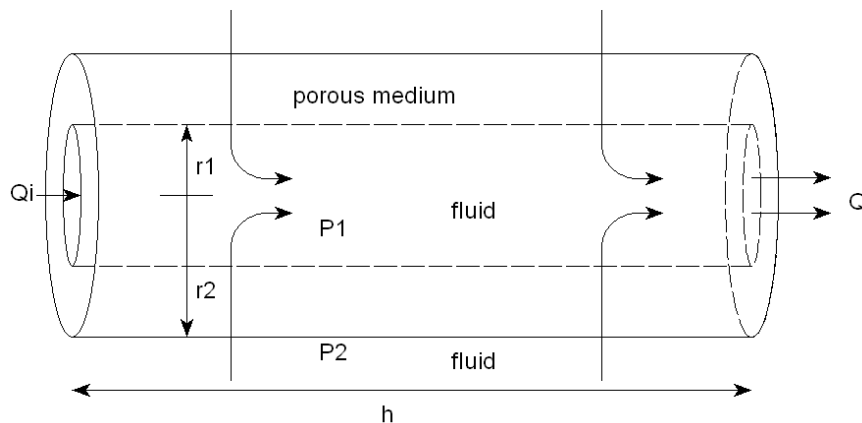


Fig. 3. Geometry of porous ceramic tube used for equation 2.

An additional consideration that must be accounted for in using this equation is the temperature of the diffused gas. There is no mention of what temperature range this equation is to be used for so it is assumed to be at or near room temperature. For our design, nitrogen will be the gas diffused through the cylinder at a temperature of approximately 1000 °C. With elevated temperatures gas density changes which in turn effects the kinematic viscosity of the fluid. This requires application of the ideal gas law to determine the nitrogen gas properties at elevated temperature before using the above equation.

At the end of the first semester, our design team had been finalizing the ceramic tube size and trying to determine permeability as well as contacting suppliers of porous ceramics. The material with greatest potential for this application was Duocel Silicon Carbide foam from ERG Materials and Aerospace Corporation. According to our advisors findings, the time for the pyrolysis reaction to occur is not directly dependent on tube length but more importantly the ratio of  $Q$  and  $Q_i$ . This ratio is adjustable in our current design scheme. With this information, we decided to pursue a ceramic tube  $24 \frac{1}{4}$  in length with an outer diameter of 3 in (similar to the size used in the original particle generator [7]). The thickness of the tube will be between  $\frac{1}{8}$  to  $\frac{1}{4}$  in, this value still being evaluated. The final thickness selected was dependent upon the flow rate and pressures from Eq. (2) as well as heat transfer considerations that will be discussed shortly.

Regarding permeability, ceramics companies define two characteristics of the foam that must be specified; relative density (porosity) and pore size. As recommended by our advisor, a pore size of 500  $\mu\text{m}$  would be considered as a starting point. The manufacturer requires this value to be in terms of pores per linear inch (PPI); a value of 50 PPI corresponding to a 500  $\mu\text{m}$  pore size. We also started with a relative density of 50%. With these values defined, a price quote was being generated by the company before winter vacation. Tube thickness was to be finalized after consultation with the ERG's design engineer as well as porosity and pore size.

Having decided on the porous ceramic inner chamber and the metal outer chamber design the remaining challenges were how to seal the ceramic tube to the metal outer chamber and what material choices were acceptable for the outer chamber. The first iteration of the ceramic/metal

chamber interface involved passing the ceramic tube through the ends of the metal chamber. The difficulty with sealing this arrangement was that all commercially available seals for high temperature applications begin to break down at 600 °C and the temperatures in the chamber would be closer to 1000 °C. Without heavy insulation, this design was unusable. The interface of hoses or pipes carrying the gas into and out of the chamber with the ceramic tube was another problem with this design. The second design iteration for sealing the ceramic tube with the steel outer chamber involved countersinking the ceramic tube into the ends of the outer chamber. This is shown in the cross-sectional view in Fig. 4.

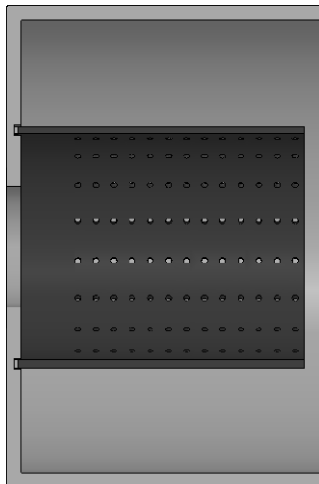


Fig. 4. Ceramic tube and metal chamber interface.

With this design, sealing was not as critical since the ceramic tube does not pass through the outer chamber. Of design concern was the thermal expansion due to high temperatures of both the metal outer chamber and the ceramic inner chamber. Our design team needed to determine the radial and longitudinal expansion of the ceramic cylinder at the end of last semester. The radial expansion is of less concern than the longitudinal expansion that would place the ceramic tube into compressive stress. Clearance would have to be machined into the end plates to allow for this expansion and room would be left for thermal insulation to be placed in the countersunk area to keep the temperature of the metal outer plate below a specific temperature. Since this insulation was compressed its thermal conductivity would be reduced so some approximation for this effect will have to be taken.

With regards to material choices for the outer chamber, high temperature metals were considered with Inconel alloys the initial choice. Upon reconsideration of the design and in an effort to reduce costs, we studied various metals rated for lower temperature ranges. Standard steel tubing sections could be used in our design if the temperature of the steel was kept below 200 °C. Our design team initially planned on lining the inner walls of the steel chamber with insulation. We designed for a tube length of 24 in, an outer diameter of 18 in, and a thickness of  $\frac{1}{4}$  in. Ideally, a steel pipe section with flanged ends would allow the use of steel endplates that could be machined to fit. Bolt patterns and sizing were yet to be specified at the end of last semester. This

allowed flexibility in how fittings for gas flow and electrical wires for the electric heating element would be passed into and out of the chamber.

The final subsystem involves the heating of the gases. Methods for heating included electric heating elements, tube furnaces, and electric arcing. The locations considered for heating the gases were outside the reaction chamber, inside the reaction chamber, or a combination of inner and outer heating with the gases being preheated outside and final heating occurring inside the reaction chamber. The heating method we pursued is electric heating elements due to their availability and wide range of geometries. Electric arcing was considered and it was determined that the heat source was too localized. For an open system reactor the localized heating source would be inefficient for pyrolyzing the steadily flowing methane gas. The tube furnace was still being considered for preheating gases or possibly using its internal heating element in our design at the end of last semester.

As for the location of the heating, our design team pursued all heating to take place in the reaction chamber to reduce the complexity of the overall system and reduce costs. The heating coils would be wrapped around the ceramic tube with wire feedthroughs passing through the ends of the reaction chamber to a temperature control device. The gases will enter the reaction chamber at room temperature. The methane will flow into the inner tube and the nitrogen will flow into the outer chamber. The nitrogen gas will pass over the heating coils and diffuse through the heated porous ceramic inner tube at the necessary temperature for the reaction to take place.

The design involves three primary heat transfer considerations. The first is the heat transfer from the heating coil radially outwards through the insulation to the outer steel chamber and ultimately the surrounding system. The second is the conductive heat transfer radially inwards through the ceramic tube, and the last is the conductive heat transfer longitudinally down the cylinder to the endplates.

It is necessary for the outer chamber to remain below 200 °C for steel to be used. This depends on the power required to heat the gas to 1000 °C, the type and thickness of the insulation, and the diameter of the outer chamber. This is a challenging problem because the gas flow conditions of the nitrogen in the outer chamber are difficult to model. The gas enters the chamber with a velocity and passes over the heating coils. This is forced convection heat transfer as given by Eq. (3)

$$q = \bar{h}A_s(T_s - T_{\infty}) \quad (3)$$

where  $\bar{h}$  is the average convection coefficient,  $A_s$  is the surface area over which heat transfer occurs,  $T_s$  is the surface temperature and  $T_{\infty}$  is the temperature of the surroundings. The study of forced convection is primarily concerned with calculating  $\bar{h}$ , depending on many fluid properties, surface geometry, and flow conditions. Both the temperature at various points in the system and the energy  $q$  are unknown, and trying to calculate the Reynolds and Nusselt number provided too many unknowns and too many assumptions. Our advisor recommended that we consider the nitrogen to be in free convection for our initial heat transfer calculations.

To simplify this even further, our advisor suggested we begin our analysis of the radial heat transfer by assuming quiescent conditions in the outer chamber. This allows the heat transfer through the nitrogen to be modeled as thermal conduction. Using Eq. (4) we first determined the heat energy of the system for a ceramic surface temperature of 1000 °C

$$q_r = \frac{T_{s,1} - T_{\infty,2}}{R_{Tot}} \quad (4)$$

where  $T_{s,1}$  is the ceramic surface temperature,  $T_{\infty,2}$  is outside fluid temperature, and  $R_{Tot}$  is total thermal resistance. The derivation of this equation from the heat diffusion equation is provided in Appendix 1. Thermal resistance for conduction is given by

$$R_{t,cond} = \frac{\ln(r_2/r_1)}{2\pi kL} \quad (5)$$

where L is the length of the cylinder and k is coefficient of thermal conductivity. Thermal resistance for convection is given by

$$R_{t,conv} = \frac{1}{2\pi r h} \quad (6)$$

where h is the coefficient of thermal convection.

The heat energy for our design was calculated using several assumptions. The most obvious assumption is treating the nitrogen gas as quiescent when it is known that the gas is forced into the system. The next assumption we made is neglecting radiation heat transfer for the present moment to simplify the initial analysis. The addition of radiation heat transfer into the system energy balance will affect our results and calculated temperatures. We also assumed a starting insulation thickness of 2 in and Thermal Ceramics superwool 607 blanket as material type due to its excellent high temperature properties. With value q from Eq. (4) the following equation allowed us to determine the temperature at various points in the chamber.

$$q = \frac{T_1 - T_2}{\frac{\ln(r_2/r_1)}{2\pi k_{N_2} L}} = \frac{T_2 - T_3}{\frac{\ln(r_3/r_2)}{2\pi k_{ins} L}} = \frac{T_3 - T_4}{\frac{\ln(r_4/r_3)}{2\pi k_{st} L}} \quad (7)$$

Using Eq. (7), equations for temperature at the inside surface of insulation, inside surface of steel outer chamber (most important), and the outside surface of the steel outer chamber were obtained. Equation (8) provides the temperature at the inside surface of the steel outer chamber

$$T_3 = T_2 - q * \frac{\ln(r_3/r_2)}{2\pi k_{ins} L} \quad (8)$$

For a constant value of q a range of insulation thickness were analyzed and the temperature of the steel inner surface was analyzed as shown in Fig. 5. Our design team needed to determine whether the outer surface of the steel chamber could be lowered to a temperature of 200 °C for a diameter of 18 in. If the insulation thickness to obtain this temperature was too large, the outer

chamber diameter would have to be increased. For larger diameters the effects of material defects, surface finish and other stress risers become a concern, especially at elevated temperature and pressure. The data used to create this graph is provided in Appendix 1.

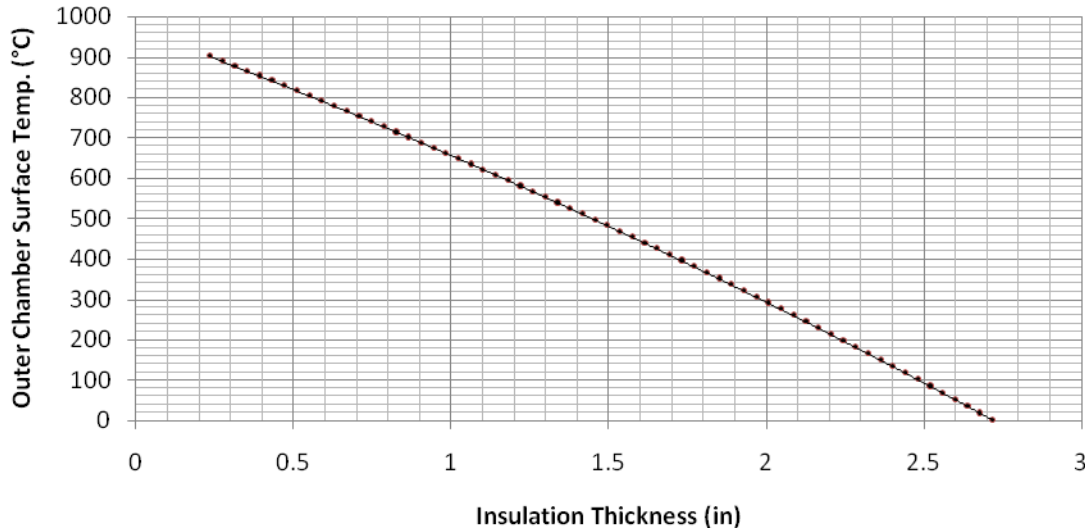


Fig. 5. Outer chamber surface temperature as a function of insulation thickness.

The results of the first iteration for radial heat transfer indicate that an insulation thickness of 2.25 in will result in an acceptable temperature of 200 °C at the surface of the steel outer chamber. Consideration must be given regarding the assumption of quiescent conditions and neglecting radiation heat transfer, both causing a higher surface temperature on the inside surfaces of the insulation and the steel chamber. This would require increasing insulation thickness and the space occupied by the heating coils must be considered as well.

The next step from this point was to determine whether our power requirement for the heating elements was obtainable from the current supplier, Kanthal, and if so will the price be within budget? The above calculation can be repeated for a constant insulation thickness and varying  $q$  if necessary to develop a range of values for power input. The addition of radiation heat transfer to the above calculation was to be completed by the design team. The same calculation will be repeated for free convection inside the outer chamber using Eq. (9)

$$q = \frac{2\pi L K_{eff} (T_1 - T_2)}{\ln(r_2/r_1)} \quad (9)$$

where all variables are as defined previously and  $K_{eff}$  is the effective thermal conductivity that will be determined using the results for  $q$  from Eq. (4). Our design team elected to perform a more involved 2-dimensional heat transfer analysis instead of using the initial model which will be discussed later.

The next heat transfer consideration was the radial conduction through the porous ceramic towards the center of the device. It must be determined whether the nitrogen will obtain a

temperature of 1000 °C before entering the reaction chamber. If the current design was incapable of achieving this, a preheat system would have to be integrated inline between gas supply and reaction chamber. The last consideration was the conductive heat transfer from the heating coils longitudinally along the porous ceramic tube. The end caps of the device must be insulated to maintain a temperature below 200 °C. This will require the heating elements to be at a distance  $x$  from the walls of the chamber and this calculation will determine the necessary distance.

#### 490B: Final Design

##### Final Design Summary:

This section provides a brief overview of the final reaction chamber design shown in Fig. 6. The following sections describe the final configuration of each part in detail. Not pictured are the temperature and gas control components

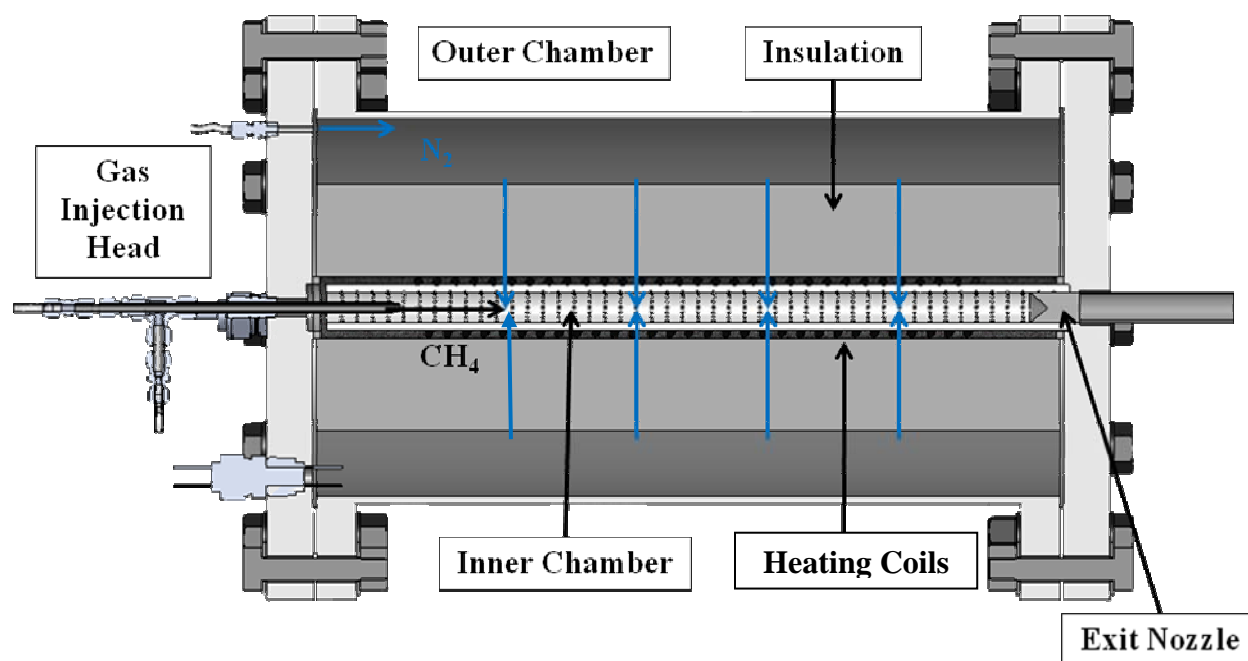


Fig. 6. Reaction chamber and gas flow detailed view

Methane gas flows through an injection head enclosed in a flow of nitrogen gas. The depth of insertion for the methane and nitrogen gases are adjustable independently. The outer chamber is constructed of steel with flanged ends and steel blinds constrained with 12 bolts. The inner chamber is porous ceramic seated in grooves machined into the end blinds. The heating coil wraps around the ceramic tube and is wrapped with blanketed insulation material. Power leads and thermocouples pass through the inlet blind using NPT feedthroughs. Nitrogen gas is injected into the outer chamber and diffuses radially inwards to the reaction site, heating during the process. The gas/ carbon mixture exits the chamber through a converging nozzle.

### Steel Chamber:

Procurement of the outer reaction chamber was the first major concern of the project after a final design was approved. The reaction chamber had to have certain qualities to fit our process and failure of any kind was not acceptable. A safety factor of 3 was used in the selection of the reaction chamber.

Initial requirements for the chamber were set to meet safety standards and also to meet the needs of the project. The first requirement was that the chamber be large enough to fit all internal components such as heating elements and insulation. The reaction chamber had to be cylindrical and able to be sealed to allow no escaping pressure. The initial design of the chamber was 18" inner diameter pipe with two blinds. The diameter had to be reduced to 12" after research into custom fabricated steel pipes with flanged ends proved to be too costly. The 12" diameter was still large enough to house all internal components. A length of 24" was finalized after calculating a maximum resonance time of one second. This length allows for complete reaction of the methane. The reaction chamber was donated by Tidelands Oil Production along with 4 Garlock gaskets, 48 nuts, and 24 bolts for securing the endplates. This helped save the project over \$800.00 in fabrication and delivery charges. The steel outer chamber is shown in Fig. 7.



Fig. 7. Steel outer chamber.

The type of metal, wall thickness, and thickness of endplates were the next major concern for this part. After some research the optimal steel chosen was ASTM a106 grade B. This type of steel was chosen due to its wide use in multiple industries and also that it maintains its material properties at 200°C. To reduce the weight of the system, a thin wall thickness of sch. 20 steel was used, approximately  $\frac{1}{4}$ " thick. The endplates of the system were 1.5" thick to ensure a minimum deflection under pressure. This was to insure no leakage of pressure while the system

is operational. The thick endplates fit our safety factor of 3 and also allow for a higher working pressure, above 120psi, incase future testing requires a higher pressure.

The system was much heavier than initially believed, over 400lbs, and attempt to reduce the weight was made. Aluminum endplates were considered but after some stress and deflection testing we found that this was not a viable option. At 150 psi the safety factor was just above 1.0, unsafe for our design considerations. These results were for static pressure loading, low cyclic fatigue from temperature cycles would decrease the safety factor further. The observed static displacement at 150 psi was 0.00476 in, above our design goal of  $\leq 0.001$  in. The results are shown in Fig. 8-9.

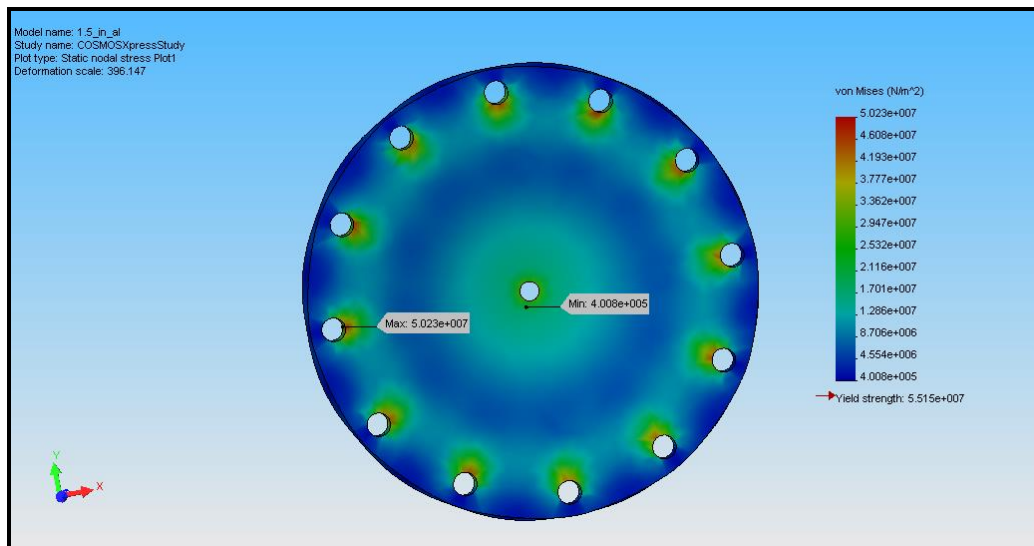


Fig. 8. 6061 Alloy 150 psi stress study.

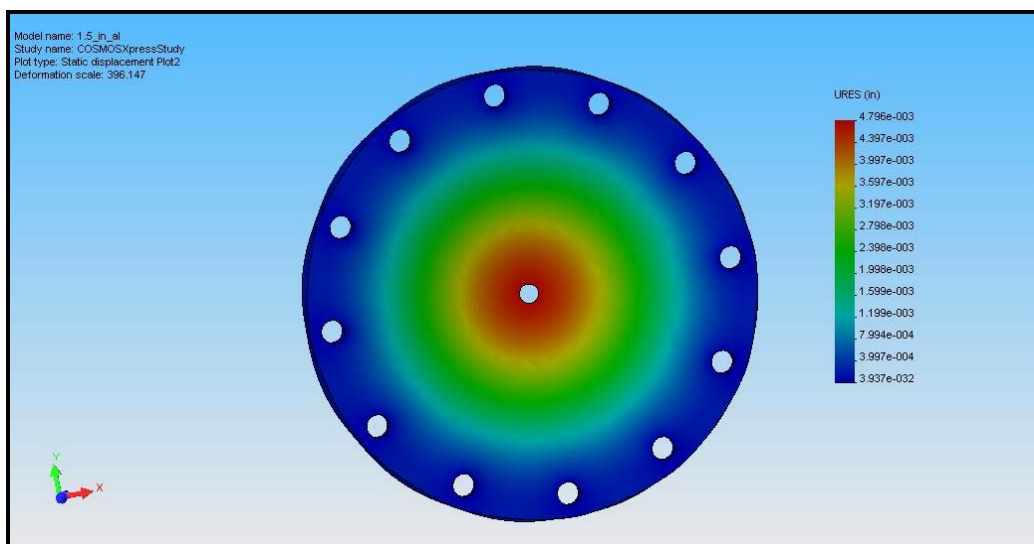


Fig. 9. 6061 Alloy 150 psi static displacement study.

The donated pipe needed to be sanded and coated to remove rust and any other particles left inside the chamber prior to assembly. The sanding was done by hand with a wire brush. The entire reaction chamber was then coated in a rust neutralizer, after sanding, which helped protect from further build up of rust. The outer wall of the chamber was then painted black along with red painted endplates.

### **Ceramic Tube:**

The inner chamber was the second major task for this project. Porous ceramics were an unknown material to the design team and presented two major challenges; properly sizing the tube and finding a supplier. The length of the ceramic tube was fixed by the outer reaction chamber dimensions at approximately 24 in. The initial size called for was 24.25 in as to allow for seating the ceramic tube into groves machined into the endplates. The diameter was an unknown factor as was wall thickness. Initially the design team pursued a 3 in inner diameter to be consistent with the adviser's early carbon generator prototype constructed of a 3 in diameter quartz tube.

Upon further discussion the design team decided to consider a 1 in inner diameter ceramic tube. Decreasing the tube diameter would decrease the power requirements for the heating coil thus reducing the cost. The smaller diameter would also position the heating coils further from the steel outer chamber and allow more room for insulation. At this point a 2 dimensional conduction model was pursued by the design team.

The model was started over winter vacation but was not completed because of other elements of the project demanding time and research. A detailed 2 dimensional conduction model was completed by a graduate student working on another component of the solar project. Results from this analysis are provided in the results section of this report. To summarize, it was found that the 1 in tube would allow for a steel surface temperature less than 200 °C, a lower heating power requirement, and a substantially lower purchase cost. Therefore the 1 in inner diameter size was chosen.

After promising initial contact with ERG Aerospace several material samples were sent to the university. A flow tunnel was constructed in order to test the pressure drop across porous ceramic samples. The results of this and pictures of the apparatus are included in the results section of this report. The ERG ceramic order fell through when the quoted delivery time and cost greatly exceeded the design teams time and budget constraints.

A new company was pursued by the name of High Tech Ceramics. They offered a comparable product at a superior price and shipping time. After conversing with the design engineers the tube selected was made of 65 PPI, 92%  $AL_2O_3$ . The tube had to be manufactured in four 6 in sections that were bonded together with Aremco cement at the ceramic factory. Having to use multiple sections glued together was not the optimal design since flow through the ceramic will be discontinuous at the bonded junctions between sections. The distance of cement saturation into the porous ceramic structure by observation was minimal so the design team was able to verify that the bonded ceramic tube will work similarly to a one piece tube. The ceramic tube used is shown in Fig. 10.



Fig. 10. Alumina inner chamber.

### **Insulation:**

The insulation of our system is essential to the safety of the project. Insulation needed to be selected that could optimally reduce heat loss from our system. Since the core operating temperatures are around  $1000^{\circ}\text{C}$ , materials that can withstand this high temperature are more expensive and harder to manufacture. Insulating the inner reaction chamber and the heating coils helps minimize the heat loss and also maintain  $200^{\circ}\text{C}$  maximum outer reaction chamber surface temperature.

The density and pressure drop across the material is needed information for mathematical analysis of the reaction chamber. The ability to flow nitrogen through the insulation is a necessity for the project. After flow testing several material samples, one was selected. The material Durablanket S was selected from Western Industrial Ceramics. The order total was \$120.79 for two rolls, 25 feet in length, 24 feet in width, and  $\frac{1}{4}$ " thickness. The thickness was determined by the minimum bending radius, an important consideration when wrapping the tube and the heating coil. The density of the material is  $6.0 \text{ lb/ft}^3$ . After the heat transfer analysis was performed an insulation thickness of 3 inches was selected as a starting point and this thickness was controlled by layering around the inner reaction chamber. Figure 11 shows the ordered insulation material.



Fig. 11. Durablanket S insulation material.

### **Heating:**

At the end of last semester internal heating was agreed upon by the design team for the method of heating the chamber. The coil was to be wrapped over the ceramic tube and wrapped in insulation. The first step was to find a heating coil material that could withstand the 1000 °C temperature. Several companies were called leading to Kanthal which offered numerous alloys that could operate at the specified temperature without breaking down. Kanthal was contacted and directed us to Industronics, a company specializing in heating coils similar to our design. After discussing design elements with their design engineers the coil material and dimensions were selected. 0.064 in (14 Gauge) Kanthal “A-F” wire, 1.75 in inner diameter coil, 16 inches in length capable of sustaining 1200W. The coil was capable of dissipating twice the amount of power as determined from calculation allowing higher temperatures to be obtained if necessary. The coil is shown in Fig. 12.



Fig. 12. Kanthal heating coil installed around outside of ceramic tube.

A Honeywell universal digital controller was ordered to power the coil. This unit has features that exceed the design requirements at the early prototype stages of the design project. But the unit is very high quality and capable of accurately controlling temperature profiles programmed in by the user using various control architectures to allow for the highest accuracy of temperature control. Two Precision Digital temperature indicators were ordered to read thermocouples that are hard wired to each unit. Three K type Inconel sheathed thermocouples were ordered from Industronics as well. Figure 13 is a front view of the controller, temperature display, and the thermocouples are in the foreground.

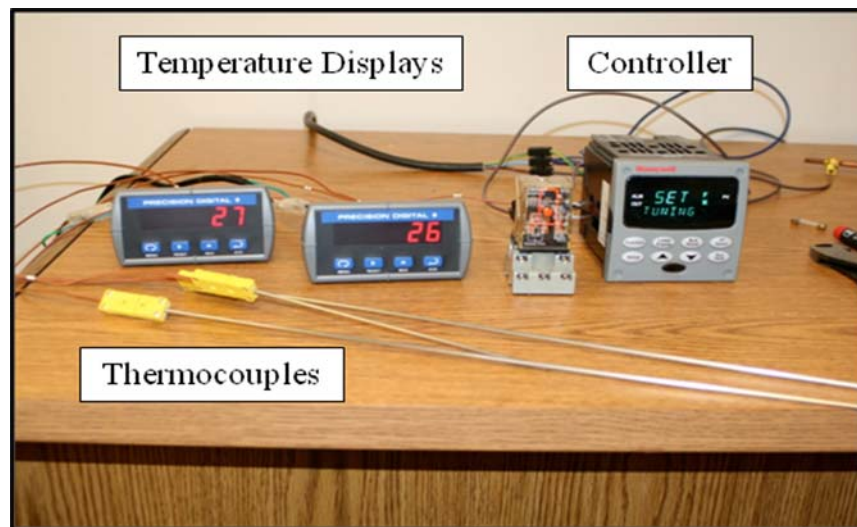


Fig. 13. Controller, temperature displays, and thermocouples.

Industronics initially wanted to put the controller and displays into a self contained housing with all input and output ports built into the back with a breaker built in in case any of the components overloaded. To save money the design adviser asked that the design team order the components separately and construct the necessary circuit to power the coil. Upon arriving, the packaging was opened to reveal only the units, no electronics were supplied nor were power cords. One of the design team members studied the manual that came with the UDC and came up with a wiring diagram. He consulted with an electrical engineer that suggested a few small changes and a trip was made to San Diego Electronic Supply to obtain all necessary components. Terminal blocks were used where possible. Inline fuses with 1 amp fast blow for the two temperature displays and UDC power supply and a 10 amp slow blow fuse were wired to protect all equipment in case of a failure. A 120 V AC 20 A mechanical relay was used. Two relay paths were used in parallel to split the 9.82 A current for the coil in order to increase the cycle life of the relay by reducing the load on each path. Power cords were obtained for each device as well.

Feedthroughs were needed to pass the power and thermocouple wires through the chamber. PAVE was contacted for power feedthroughs. After several repeated attempts the order was placed and the items arrived. Omega was contacted for an 8 wire K type thermocouple feedthrough. These items were wired into the overall circuit and tested for functionality before any machining was performed on the steel blinds. Figure 14 shows the final wiring arrangement for the electronics.

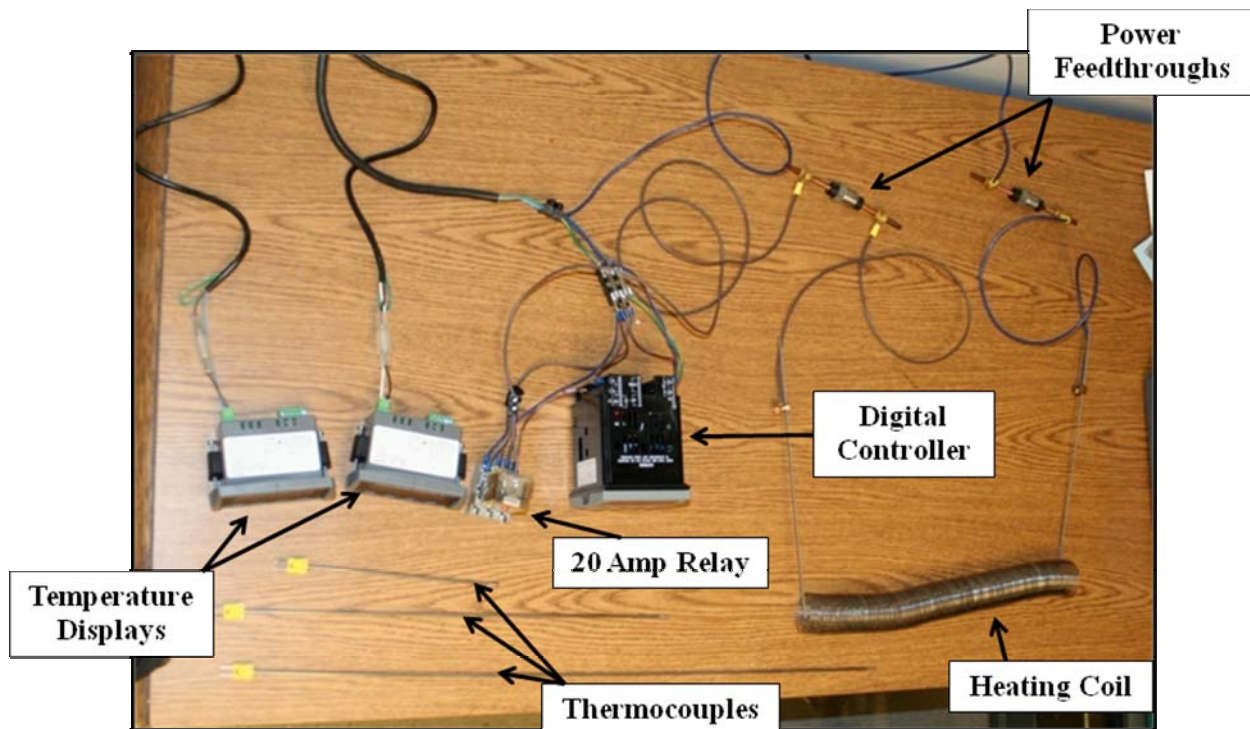


Fig. 14. Electrical system wiring setup.

The wiring of the system was more involved than initially expected. There was insufficient time to panel mount the components or place them in an enclosure. Therefore, EXTREME CAUTION

must be exercised around the open fuse blocks, feedthroughs, and exposed metal wires when the unit is on. Nearly 10 amps of current pass through the coil and could prove fatal.

Programming of the unit is currently ongoing.

### Gas Control:

Gas pressure and flow rate was a deliverable of our project. The two gases used for this project are methane and nitrogen. These two gases are controlled by various subsidiary components which help maintain constant pressure and flow rates. The supply of the gasses is initially controlled by two Airgas pressure regulators which are used to control gas pressure. Three Alicat mass flow controllers are used to control gas flow rates and ratios. Since optimal gas mixture is not known at this point in the project, the ability to control and manipulate the mixture is important for fine tuning carbon production during trial runs. Figure 15 shows a mass flow controller and pressure regulator.

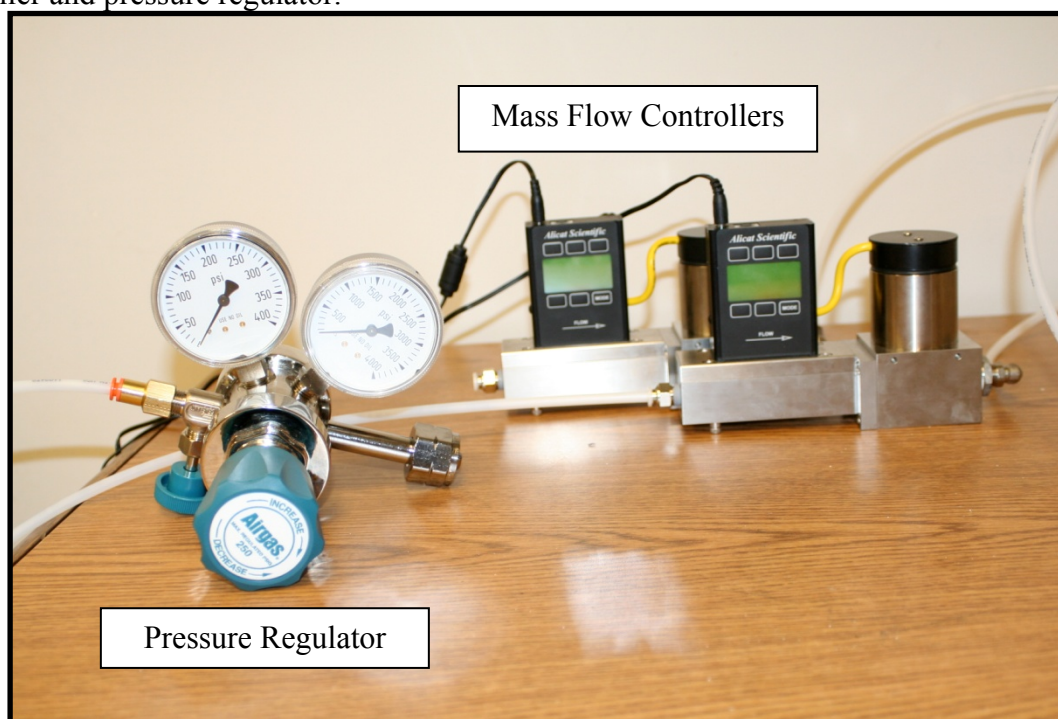


Fig. 15. Gas control system

### Injection Head:

At the beginning of the second semester of the senior design project the methane injection into the inner reaction chamber was of concern. Initially methane gas was going to be input into the system through a NPT fitting. At the advice of project advisors it was decided that methane would be injected into the system through an injection head of adjustable depth of insertion into the inner chamber. The purpose was to allow maximum flexibility in the design since it was unknown at this point where the ideal insertion point of methane should be.

Initial design ideas called for a bored through fitting to pass a stainless steel tube into the inner chamber. The methane gas would flow through the tube and the depth of insertion could be controlled by using an NPT fitting with nylon ferrules. Upon loosening the fitting's locknut the stainless tube could be physically moved to any depth into the chamber.

Building upon this idea the design team chose to inject nitrogen in with the methane into the inner reaction chamber. Multiple design iterations yielded a coaxial tube arrangement that would allow methane gas to flow down a center stainless tube with nitrogen gas flowing outside of the stream in a larger diameter stainless tube. This design proved beneficial for initial testing purposes because it further safeguards against methane reacting prematurely in the nozzle.

This design also allowed for the depth of insertion of the methane injection tube and nitrogen methane tube to be adjusted independently. Combined with control of the injected methane/nitrogen gas mixture this design yielded maximum flexibility for testing purposes. The final design injection head and a detailed view of the coaxial gas injection system is shown in Fig. 16.

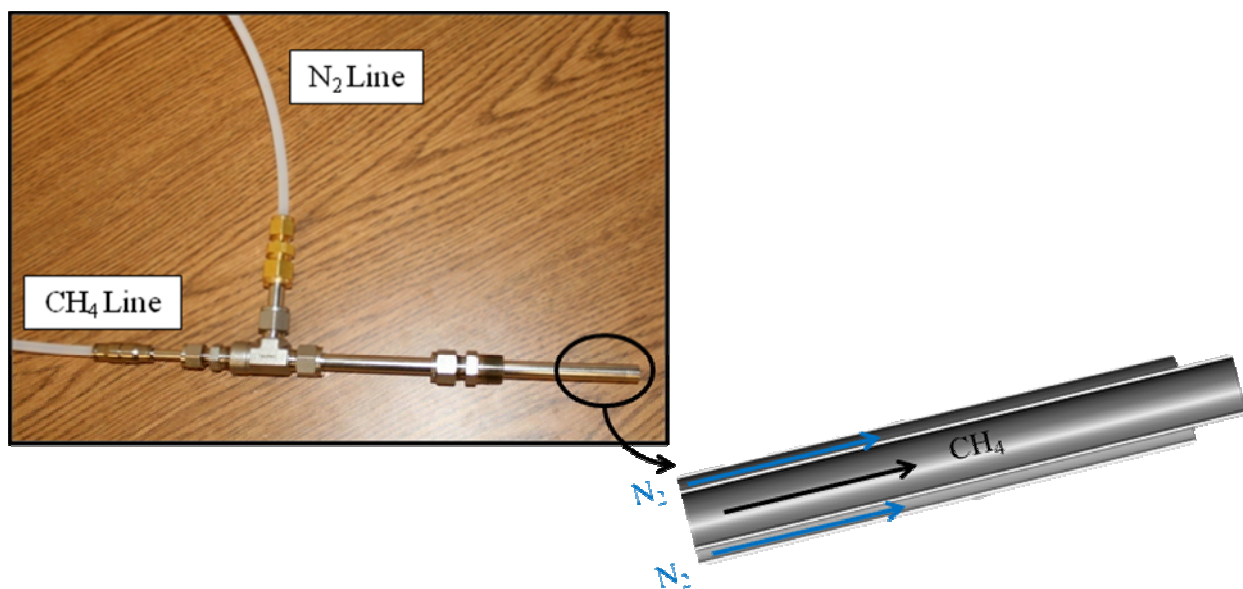


Fig. 16. Coaxial gas injection head detail.

For further understanding of the temperature distribution inside the reaction chamber to assist future students with modeling the system as well as operating it a variation of the existing injection head was designed. The latest iteration allows for a thermocouple to be passed coaxially through the inner stainless steel tube within the methane gas flow. The depth of the thermocouple can be controlled to allow temperatures to be recorded at the reaction chamber exit and various distances along the length. Figure 17 shows the final injection head design.

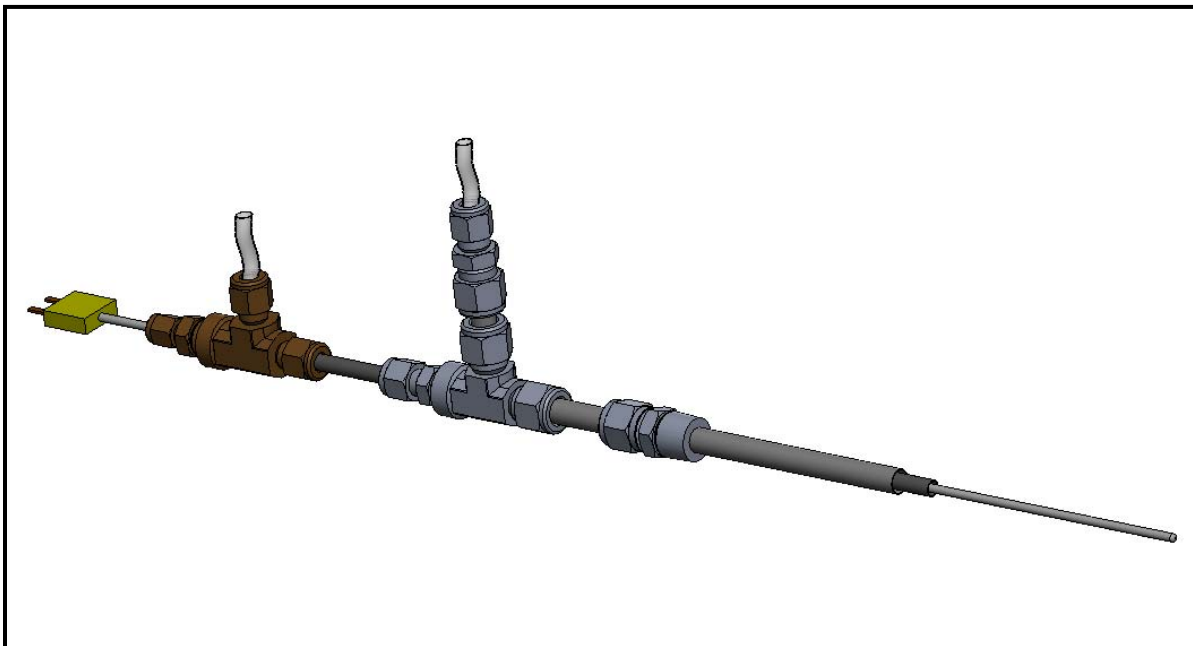


Fig. 17. Experimental design of injection head.

This configuration of the injection head will be used for information gathering purposes only. The thermocouple and brass run Tee (left Tee in Fig.17.) will be used for trial runs when methane is either not running through the injection head or for short durations of methane flow. The thermocouple probe will be directly in the center of the reaction chamber at the main site of pyrolysis. Carbon build up is a concern with this design operating in steady state conditions and is against one of the project specifications, minimal disassembly for cleaning.

#### **Nozzle:**

The nozzle was created to help maintain pressure in the chamber and also to prevent back flow into the system. The emissions of the particle generator not only produce carbon but also hydrogen molecules which are very volatile and could possibly cause an explosion if back flow of air went into the reaction chamber. To combat this problem several solutions were considered but the nozzle design was most applicable to our design. A standard check valve could not be used to increase pressure and prevent back flow since carbon build up would be a concern.

The nozzle is 1.6" in length and has an outer diameter of 1". The throat diameter is 0.1" and has a throat length of 1". Turbulent flow was assumed in nozzle throat. Table 2 in the appendix shows various throat diameters and their corresponding pressure drops. The 0.1" diameter throat was optimal for our design but with a nozzle design different pressures can be reached simply by changing the diameter of the throat instead of having to change the flow rates. The current pressure drop with a throat diameter of 0.1" is 50.25 psi. The exit NPT fitting and nozzle are shown in Fig. 18.



Fig. 18. Exit NPT fitting and nozzle.

### **Inlet and Exit Blinds/ Machining:**

The machining of the blinds was a major undertaking and required precision when creating the tapped holes. The machining could not begin until delivery of the inner reaction chamber and its final length was known. With the help by Mike Lester the machining of the end blinds proved to not be very complicating. Stepped sections of the initial groove were removed after talking with mike to simplify the machining process.

The inlet blind was the most complicated and had five tapped holes. The inlet blind needed an injection point at the center, a nitrogen injection point, two power feed throughs, and a thermocouple feed through. This translates into a center injection point of 3/8" NPT, three 1/2" NPT, and one 1/4" NPT tapped holes. The location of the 1/2" and 1/4" holes do not matter as long as there are between the wall of the outer reaction chamber and insulation. Drawings of all machined items are included in the Drawings section of this report.

The exit blind was considerably simpler to machine since only one tapped hole was currently needed. The 1" NPT tapped hole is essential to keeping our process clean. The carbon build up would be significant if a lip was created.

The Blinds will have a 1.6" inner diameter 1/4" thick metal rings welded onto the inside of the blinds to provide a lip for the inner reaction chamber. This "lip" was designed to hold the tube in place when thermal expansion and contraction occurs.

## Results

### Permeability Testing:

Permeability is the measurement of a permeable materials ability to transmit fluid flow. The design team needed this knowledge to model the flow of gases as they enter the reaction chamber. It was also necessary to determine if the pressure drop across the ceramic and insulation materials was sufficient enough to enable uniform gas flow along the entire length and circumference of the ceramic tube. The analogy to this is a garden sprinkler that has multiple holes in it along its length. The pressure drop across each hole has to be greater than the pressure drop across the length of the sprinkler or else all of the water would flow out the first hole resulting in poor water dispersion. For our design to be successful, the gas must form a uniform boundary layer around the entire inner surface of the inner ceramic chamber to prevent carbon build up.

To perform this testing our team had to design and construct a flow tunnel. Unfortunately the material samples were of different sizes so fixtures had to be made that would clamp into our flow tunnel to allow testing of each. The components were machined a liquid manometer was used to measure the pressure drop across the samples. Figures 19 and 20 illustrate the test setup.

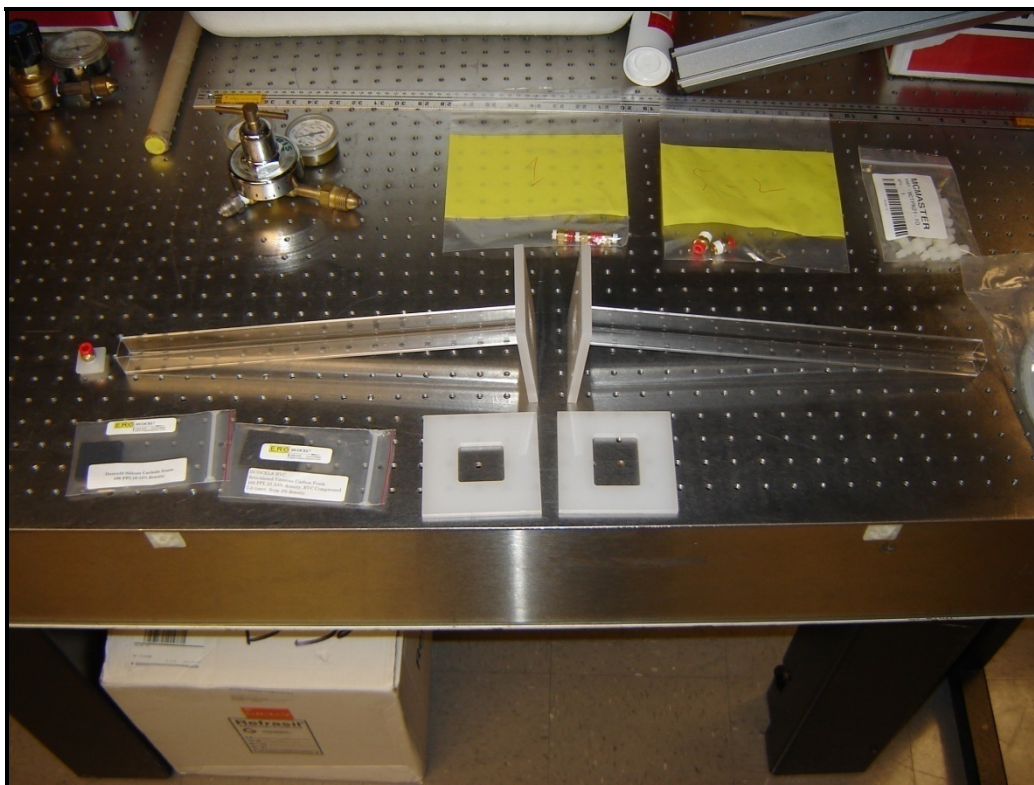


Fig. 19. Flow tunnel components.



Fig. 20. Test setup including mass flow controller and liquid manometer (Gas was replaced with nitrogen cylinder)

### Calculations

The equation used to calculate permeability is Darcy's law. It is stated as

$$Q = \frac{-kA}{\mu} * \frac{\Delta P}{L} \quad (10)$$

where  $Q$  is flow rate in  $\text{in}^3/\text{s}$ ,  $k$  is permeability in  $\text{in}^2$ ,  $A$  is cross-sectional area of flow in  $\text{in}^2$ ,  $\mu$  is kinematic viscosity in  $\text{lbm}/\text{in}^2\text{s}$ ,  $\Delta P$  is the pressure drop across the sample in psi, and  $L$  is the length over which the pressure drop is acting over in in. Rearranging Eq. (1) to solve for  $k$  and absorbing the minus sign into the  $\Delta P$  gives,

$$k = \frac{Q\mu}{A} * \frac{L}{\Delta P} \quad (11)$$

This equation will be used to calculate permeability for the material samples tested.

#### Conversion Factors

The mass flow controller uses the units of Standard Liters per Minute (SLPM) which are actually units of volumetric flow. To obtain mass flow the density of the gas would be needed. In our case volumetric flow rate is used for calculating Q but the units must be changed to  $\text{in}^3/\text{s}$ . The following conversion is used:

$$\left(\frac{1 \text{ L}}{\text{min}}\right) * \left(\frac{.001 \text{ m}^3}{1 \text{ L}}\right) * \left(\frac{\text{min } 0.6886 \text{ ft}^3}{\text{m}^3 \text{ min}}\right) * \left(\frac{(12 \text{ in})^3}{1 \text{ ft}^3}\right) \quad (12)$$

$$\frac{1 \text{ L}}{\text{min}} = \frac{0.001418 \text{ m}^3}{\text{s}} \quad (13)$$

The last conversion that must be account for is necessary when using English units. Solving Eq. (2) will result in units that are inconsistent with literature for permeability.

$$\frac{\text{in}^3}{\text{s}^2} * \frac{\text{lbm}}{\text{lb}_f} \quad (14)$$

which must be manipulated with the following conversion factor to obtain units of  $\text{in}^2$

$$1 \text{ lb}_f = 386.088 \frac{\text{lbm in}}{\text{s}^2} \quad (15)$$

#### $\Delta P$ Across Samples

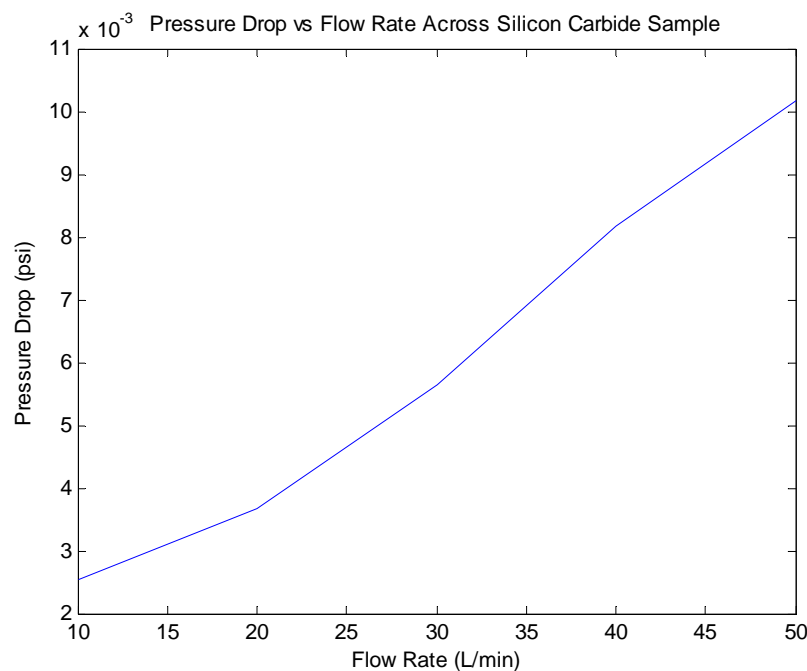


Fig. 21. Silicon Carbide Foam, 100 PPI, 10-15% density.

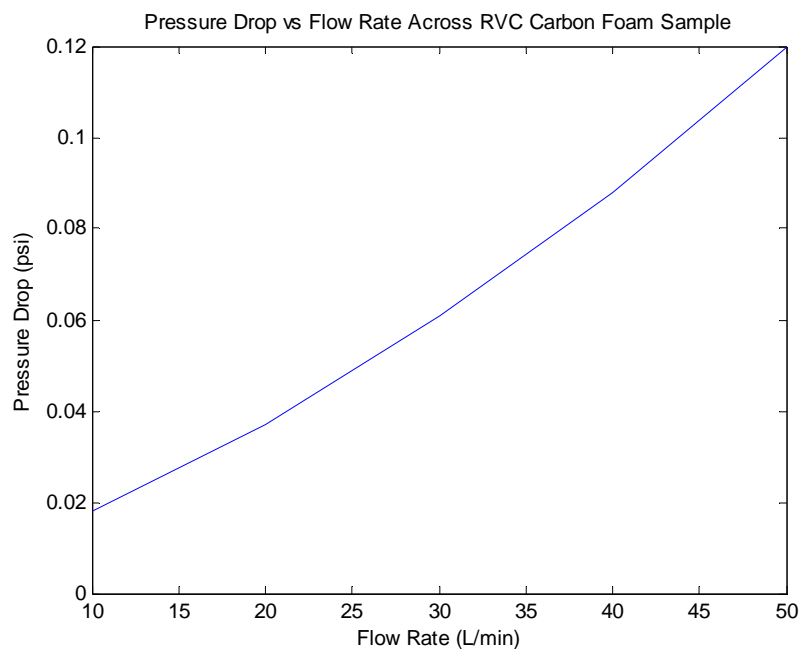


Fig. 22. Reticulated Vitreous Carbon Foam 100 PPI, 21 - 24% density, RVC compressed 7 - 8 times from 3% density.

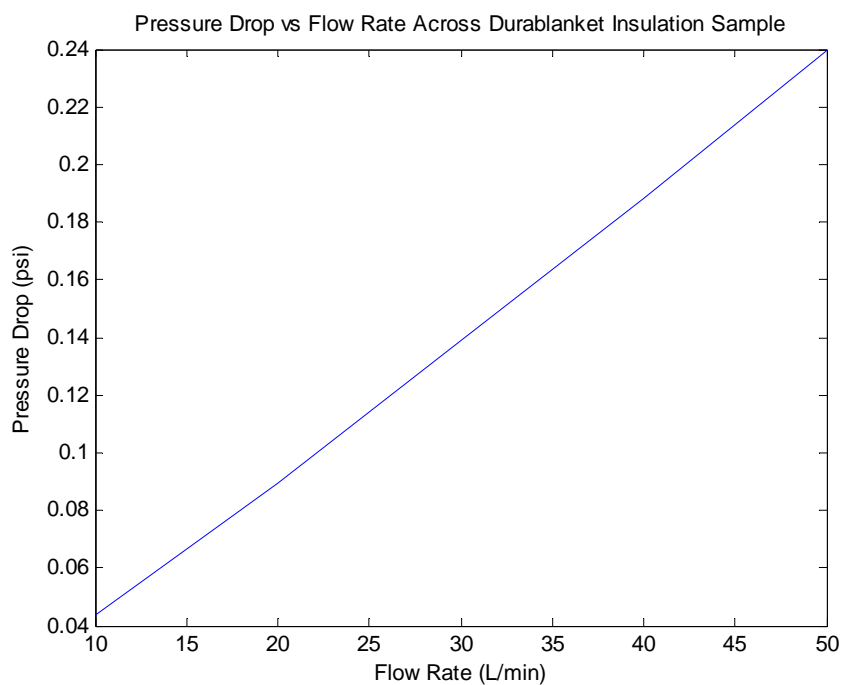


Fig. 23. PS 6448 Durablanket - S 6# - 1/2".

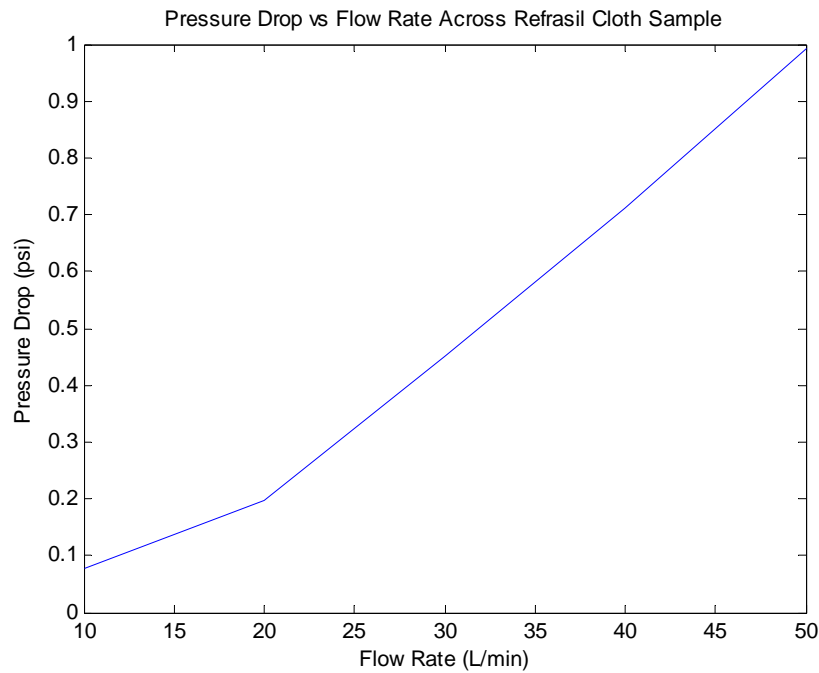


Fig. 24. Refrasil UC100-96 Standard Woven Fabric

Excel data is provided in Appendix A.

### Heat Transfer:

A more detailed heat transfer model was begun by our team over winter vacation in an attempt to perform a finite difference analysis in two-dimensions to reduce the number of assumptions and increase the accuracy of the analysis. The task was not completed due to time restrictions working on other aspects of the project so the task was finished by a graduate student. At this point in the design a 1 in and 3 in inner reaction chamber were being considered. Both were modeled using the improved 2-D model and power requirements were determined for each condition. The graphical results are provided in Fig. 25 and 26. The MATLAB code used to generate the plots is provided in Appendix C.

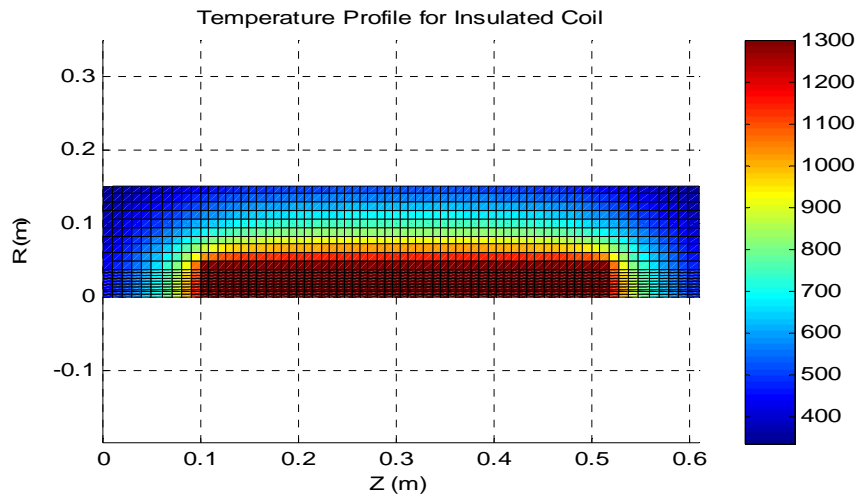


Fig. 25. 3 in tube heat transfer analysis. Temperatures in Kelvin. Credit Steve Ruther.

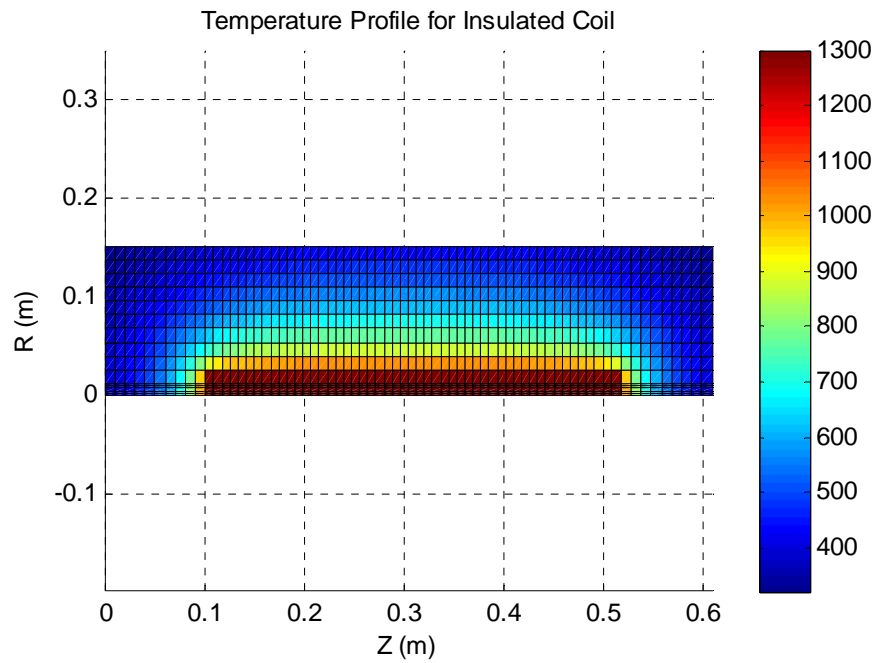


Fig. 26. 1 in tube heat transfer analysis. Temperatures in Kelvin. Credit Steve Ruther, the man.

From these results it was determined that the 3 in tube had a surface temperature of just over 200 °C for an insulation thickness of 3 in. The power required to maintain this temperature was determined to be 950 W. For the 1 in tube the surface temperature was below 200 °C for an insulation thickness of 3 in. The power required to maintain this temperature was determined to be 600 W. Our design team decided to use the 1 in tube for reduced cost in terms of the tube itself and the required heating element.

### **Bench Run of Heating System**

The heating system was bench tested up to 900 °C. The controller was not programmed so the 120 V main relay was manually closed. Temperatures were recorded at the center of the heating coil through one layer of insulating, near the end of the heating coil through one layer of insulation, and in the center of the ceramic tube at the ceramics surface. It was observed that the bonded cement regions took longer to heat to 900 °C and remained cooler for approximately 5 minutes after the ceramic surface had reached 900 °C. For pyrolysis runs the chamber should be allowed to operate at set temperature for 5 minutes to allow ceramic and cement to obtain the steady state target temperature. The ceramic tube wrapped with heating coil and insulation as well as the Inconel thermocouples are shown in Fig. 27.

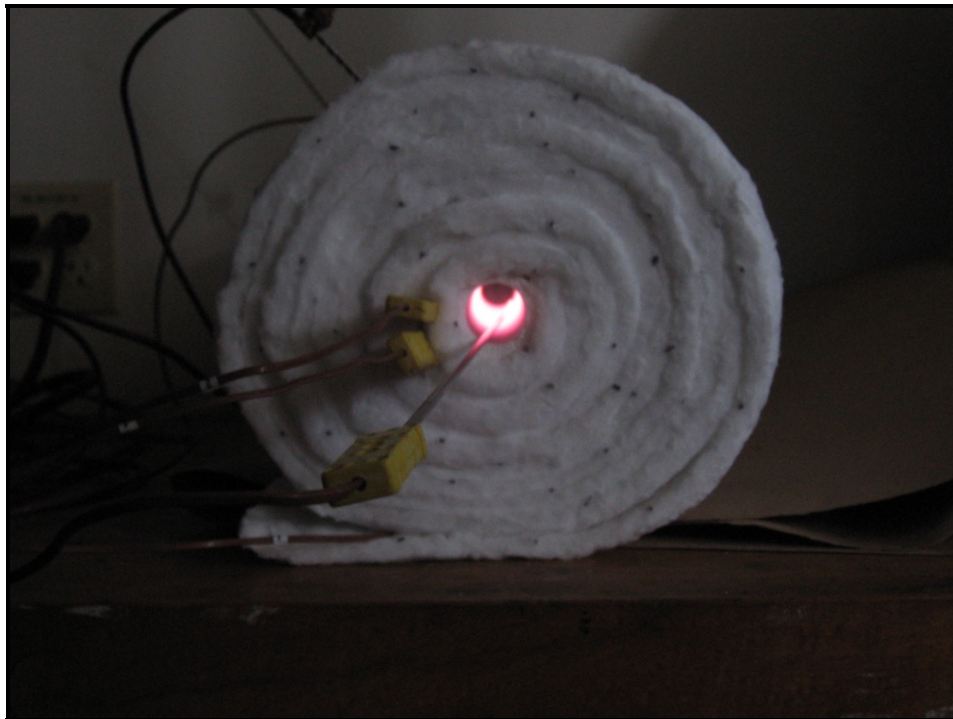


Fig. 27. Bench test of heating system. Temperature is 900 °C.

**Conclusion**

The small carbon particle generator is close to being ready for testing but a few things need to be addressed before full testing can begin. The chamber itself needs to be mounted on some sort of frame so that the testing can be conducted vertically. An internal mount for the inner reaction chamber is recommended as well to help improve loading and disassembly of the chamber. The exit of the gas configuration still needs to be assessed and modified to fit the particle scatterometer to measure exiting particles. This is still an unknown since the device is still not in our possession. The blinds need to be painted and recoated with antirust spray before full assembly. This is mainly for aesthetics of the project. The final design configuration of the generator is flexible and appears to be on the right track for full time testing that will be conducted at a later time. A dry bench test of the heating system has been preformed already with the inner reaction chamber wrapped in the insulation and heating coils. The system was powered up to 1000°C and the insulation top layer was cool enough to place a hand on top of it while sustaining the core temperature. The initial results look promising and more testing must be conducted over summer. Much was learned from this research project and the knowledge gained was invaluable. Hopefully full testing will occur in the next few weeks and the design team members will be present.

**Acknowledgements**

The Small Carbon Particle Generator team would like to thank:

**Sponsor:**

- Google.org

**Advisors:**

- Dr. Fletcher Miller
- Dr. Arlon Hunt

**Special Thanks:**

- Mike Lester for machine shop help.
- Steve Ruther for 2 dimensional conduction program.

**Companies:**

- Industronics
- Hi Tech Ceramics
- Tideland Oil Production
- Swagelok
- San Diego Electronic Supply
- Omega
- PAVE
- McMaster Carr
- Marshall's Hardware

## References

1. "Pyrolysis" Definition, Dictionary.com, <http://dictionary.reference.com/browse/pyrolysis> (3 Nov 2008).
2. Hunt, A., J., "Small Particle Heat Exchangers," Lawrence Berkeley Laboratory, LBL 7841, 1, 19-20.
3. Net Generation by Energy Source by Type of Producer, Energy Information Administration, 2007, <http://www.eia.doe.gov/cneaf/electricity/epa/epat1p1.html>, (3 Nov 2008).
4. Reiff, P., H., The Sun-Earth Connection, 1999, <http://space.rice.edu/IMAGE/livefrom/sunearth.html>, (3 Nov 2008).
5. Becker, M., and Meinecke, W., and Geyer, M., and Trieb, F., and Blanco, M., and Romero, M., and Ferrière, A., 2000, "Solar Thermal Power Plants," 3-4
6. Albright, L, Crynes, B, & Corcoran, W (1983). Pyrolysis: Theory and Industrial Practice. New York: Academic Press.
7. Hunt, A, Evans, D. Phase I Report: The Design and Construction of a High Temperature Gas Receiver Utilizing Small Particles as the Heat (SPHER). Solar Group: Energy & Environment Division Lawrence Berkeley Laboratory.
8. Stewart, Bird (1960). Transport Phenomena. Pg. 151



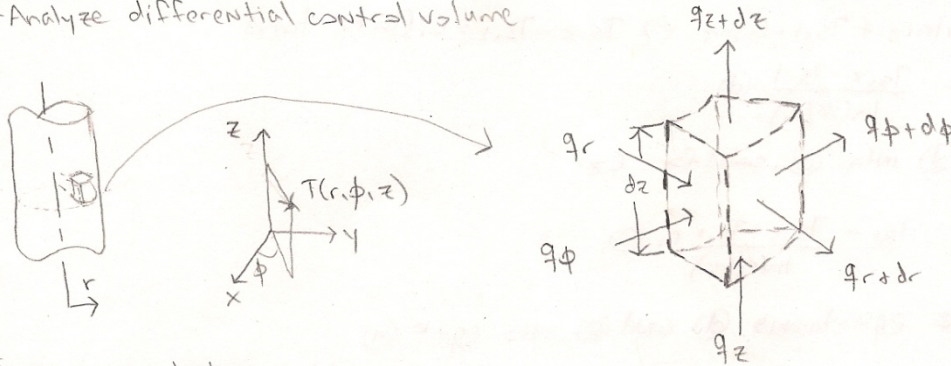
Derivation of Fourier's Law for Cylindrical Coordinates from the General Heat Diffusion Equation

One-Dimensional Steady-State Conduction

- Begin with heat diffusion equation
- General Form: Cartesian Coordinates

$$\frac{\partial}{\partial x} \left( k \frac{\partial T}{\partial x} \right) + \frac{\partial}{\partial y} \left( k \frac{\partial T}{\partial y} \right) + \frac{\partial}{\partial z} \left( k \frac{\partial T}{\partial z} \right) + \dot{q} = \rho c_p \frac{\partial T}{\partial t} \quad (1)$$

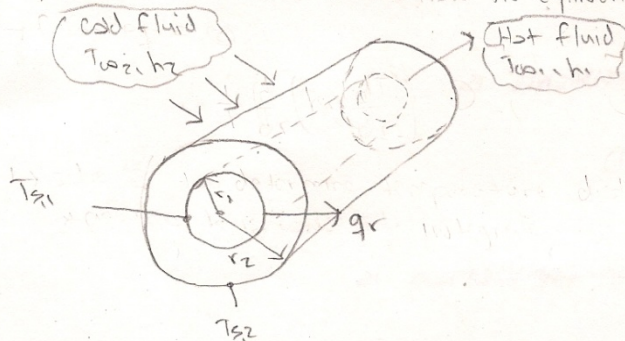
- Cylindrical Coordinates
- + Analyze differential control volume



- From energy balance:
- ↳ General form of heat equation for cylindrical coordinates

$$\frac{1}{r} \frac{\partial}{\partial r} \left( kr \frac{\partial T}{\partial r} \right) + \frac{1}{r^2} \frac{\partial}{\partial \phi} \left( k \frac{\partial T}{\partial \phi} \right) + \frac{\partial}{\partial z} \left( k \frac{\partial T}{\partial z} \right) + \dot{q} = \rho c_p \frac{\partial T}{\partial t} \quad (2)$$

- For steady, one-dimensional conduction in cylindrical coordinates



- For one-dimensional steady-state conduction in cylindrical coordinates
- ↳ From eq 2

$$\frac{1}{r} \frac{d}{dr} \left( kr \frac{dT}{dr} \right) = 0 \quad (3)$$

- ↳ Determine temperature distribution in cylinder
- + assume k is constant, integrate twice

$$T(r) = C_1 \ln r + C_2 \quad (4)$$

Fig. 7. Detailed drawing of steel outer chamber with current specifications.

- Apply these conditions to eqn (4)

$$T_{s,1} = C_1 \ln r_1 + C_2 \quad (a)$$

$$T_{s,2} = C_1 \ln r_2 + C_2 \quad (b)$$

- From (a)

$$C_2 = T_{s,1} - C_1 \ln r_1 \quad (c)$$

- Substitute into (b), solve for  $C_1$

$$T_{s,2} = C_1 \ln r_2 + T_{s,1} - C_1 \ln r_1 \Rightarrow T_{s,2} - T_{s,1} = C_1 (\ln r_2 - \ln r_1)$$

$$C_1 = \frac{T_{s,2} - T_{s,1}}{\ln(r_2/r_1)} \quad (d)$$

- Plug (d) into (c), solve for  $C_2$

$$C_2 = T_{s,1} - \frac{T_{s,2} - T_{s,1}}{\ln(r_2/r_1)} r_1 \quad (e)$$

- Substitute equations (d) and (e) into eqn (4)

$$T(r) = \frac{T_{s,1} - T_{s,2}}{\ln(r_1/r_2)} \ln\left(\frac{r}{r_2}\right) + T_{s,2} \quad (5)$$

- Using temperature distribution (eqn 5) w/ Fourier's Law ( $q_r = -kA \frac{dT}{dr}$ )

$$q_r = \frac{2\pi L k (T_{s,1} - T_{s,2})}{\ln(r_2/r_1)} \quad (6)$$

- From eqn (6), the thermal resistance is

$$R_{t, \text{cond}} = \frac{\ln(r_2/r_1)}{2\pi L k} \quad (7)$$

- Similarly, thermal resistance for convection is

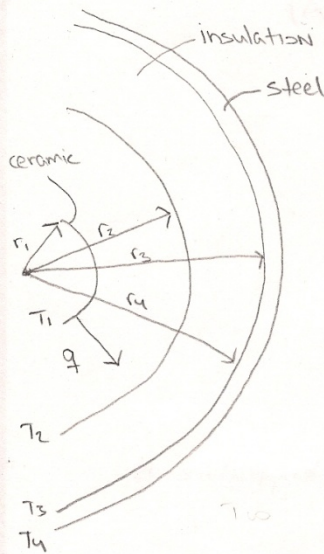
$$R_{t, \text{conv}} = \frac{1}{2\pi r L h} \quad (8)$$

$$\Rightarrow q_r = \frac{T_{\infty,1} - T_{\infty,2}}{R_{TOT}}$$

\* Using the assumption of quiescent conditions in the reaction chamber, initial temperatures at various points in the system can be analyzed.

1st Approximate quiescent fluid conditions

↳ Allows us to assume conduction through N<sub>2</sub> gas

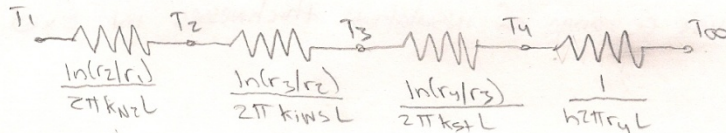


Assume:

- Radiation effects not considered
- $T_2 = 700^\circ\text{C}$
- Steel 1/4" thick
- Insulation 2" thick
- Value for  $k_{ins}$  taken at  $1095^\circ\text{C}$
- Surface of ceramic at  $1000^\circ\text{C}$

Atm Air  
 $T_{\infty} = 25^\circ\text{C}$   
 $h = 15 \text{ W/m}^2\cdot\text{K}$

- $k_{st} = 60.5 \text{ W/m}\cdot\text{K}$
- $k_{ins} = 0.329 \text{ W/m}\cdot\text{K}$
- $k_{N_2}(700^\circ\text{C}) = 63.35 \text{ W/m}\cdot\text{K}$
- $r_1 = 1.5 \text{ in} = 0.0381 \text{ m}$
- $r_2 = \text{Variable}$
- \* Start at:  
 $6.75 \text{ in} = 0.17145 \text{ m}$
- $r_3 = 8.75 \text{ in} = 0.2225 \text{ m}$
- $r_4 = 9 \text{ in} = 0.2286 \text{ m}$
- $L = 24 \text{ in} = 0.6096 \text{ m}$



- solve for q

$$q = \frac{T_1 - T_{\infty}}{R_{tot}} = \frac{T_1 - T_{\infty}}{\frac{\ln(r_2/r_1)}{2\pi k_{N_2} L} + \frac{\ln(r_3/r_2)}{2\pi k_{ins} L} + \frac{\ln(r_4/r_3)}{2\pi k_{st} L} + \frac{1}{h 2\pi r_4 L}}$$

$$= \frac{1000 - 25}{\frac{\ln(0.17145/0.038)}{2\pi(63.35)(0.6096)} + \frac{\ln(0.2225/0.17145)}{2\pi(0.329)(0.6096)} + \frac{\ln(0.2286/0.2225)}{2\pi(60.5)(0.6096)} + \frac{1}{(15)(2\pi)(0.2286)(0.6096)}}$$

$q = 3370.39 \text{ W} = 3.37 \text{ kW}$

$$q = \frac{T_1 - T_2}{\ln(r_2/r_1)} = \frac{T_2 - T_3}{\ln(r_3/r_2)} = \frac{T_3 - T_4}{\ln(r_4/r_3)} = \frac{T_4 - T_{\infty}}{\frac{1}{h 2\pi r_4 L}}$$

• Can now solve for  $T_2, T_3, T_4$

$$T_2 = T_1 - q \left( \frac{\ln(r_2/r_1)}{2\pi k_{ins} L} \right) = 1000 - (3370.39 \text{ W}) \left( \frac{\ln(0.17145/0.0381)}{2\pi(63.35 \text{ W/m}\cdot\text{K})(0.6096 \text{ m})} \right)$$

$$T_2 = 979.108^\circ\text{C}$$

$$T_3 = T_2 - q \left( \frac{\ln(r_3/r_2)}{2\pi k_{ins} L} \right) = 979.108 - (3370.39) \left( \frac{\ln(0.2225/0.17145)}{2\pi(0.379)(0.6096)} \right)$$

$$T_3 = 282.012^\circ\text{C}$$

$$T_4 = T_3 - q \left( \frac{\ln(r_4/r_3)}{2\pi k_{st} L} \right) = 282.012 - (3370.39) \left( \frac{\ln(0.2286/0.2225)}{2\pi(60.5)(0.6096)} \right)$$

$$T_4 = 281.614^\circ\text{C}$$

\* For the assumption of 2 in insulation thickness, the steel temperature is  $> 200^\circ\text{C}$ .

• Keeping  $q$  fixed, evaluate a range of insulation thicknesses in Excel.

Table 1. Values used to create Fig. 4

| Constants |        |        |        |         |           |                |                    |             |           |         |
|-----------|--------|--------|--------|---------|-----------|----------------|--------------------|-------------|-----------|---------|
| R1 (m)    | R3 (m) | R4 (m) | L (m)  | T2 (°C) | Tinf (°C) | Ksteel (W/m²K) | Insulation (W/m²K) | RNG (W/m²K) | h (W/m²K) | q (W)   |
| 0.0381    | 0.225  | 0.2286 | 0.6096 | 1000    | 25        | 60.5           | 0.329              | 63.35       | 15        | 3370.39 |

| Variable of Interest |                           |
|----------------------|---------------------------|
| r2 (m)               | Insulation Thickness (in) |
| 0.156                | 2.71653543                |
| 0.157                | 2.677165352               |
| 0.158                | 2.637795273               |
| 0.159                | 2.598425194               |
| 0.16                 | 2.559055116               |
| 0.161                | 2.519685037               |
| 0.162                | 2.480314958               |
| 0.163                | 2.440944879               |
| 0.164                | 2.401574801               |
| 0.165                | 2.362204722               |
| 0.166                | 2.322834643               |
| 0.167                | 2.283464565               |
| 0.168                | 2.244094486               |
| 0.169                | 2.204724407               |
| 0.17                 | 2.165354329               |
| 0.171                | 2.12598425                |
| 0.172                | 2.086614171               |
| 0.173                | 2.047244092               |
| 0.174                | 2.007874014               |
| 0.175                | 1.968503935               |
| 0.176                | 1.929133856               |
| 0.177                | 1.889763778               |
| 0.178                | 1.850393699               |
| 0.179                | 1.81102362                |
| 0.18                 | 1.771653542               |
| 0.181                | 1.732283463               |
| 0.182                | 1.692913384               |
| 0.183                | 1.653543305               |
| 0.184                | 1.614173227               |
| 0.185                | 1.574803148               |
| 0.186                | 1.535433069               |
| 0.187                | 1.496062991               |
| 0.188                | 1.456692912               |
| 0.189                | 1.417322833               |
| 0.19                 | 1.377952755               |
| 0.191                | 1.338582676               |
| 0.192                | 1.299212597               |
| 0.193                | 1.259842518               |
| 0.194                | 1.22047244                |
| 0.195                | 1.181102361               |
| 0.196                | 1.141732282               |
| 0.197                | 1.102362204               |
| 0.198                | 1.062992125               |
| 0.199                | 1.023622046               |
| 0.2                  | 0.984251967               |
| 0.201                | 0.944881889               |
| 0.202                | 0.90551181                |
| 0.203                | 0.866141731               |
| 0.204                | 0.826771653               |
| 0.205                | 0.787401574               |
| 0.206                | 0.748031495               |
| 0.207                | 0.708661417               |
| 0.208                | 0.669291338               |
| 0.209                | 0.629921259               |
| 0.21                 | 0.59055118                |
| 0.211                | 0.551181102               |
| 0.212                | 0.511811023               |
| 0.213                | 0.472440944               |
| 0.214                | 0.433070866               |
| 0.215                | 0.393700787               |
| 0.216                | 0.354330708               |
| 0.217                | 0.31496063                |
| 0.218                | 0.275590551               |
| 0.219                | 0.236220472               |

| Results     |             |        |
|-------------|-------------|--------|
| T2          | T3          | T4     |
| 980.4197849 | 0.861189441 | 0.6303 |
| 980.3310293 | 17.86261114 | 17.632 |
| 980.2428372 | 34.75698658 | 34.525 |
| 980.1552016 | 51.54297787 | 51.312 |
| 980.0681153 | 68.22462149 | 67.994 |
| 979.9815717 | 84.80232897 | 84.571 |
| 979.895564  | 101.2773875 | 101.05 |
| 979.8100855 | 117.6510603 | 117.42 |
| 979.7251298 | 133.9245878 | 133.69 |
| 979.6406906 | 150.0991874 | 149.87 |
| 979.5567616 | 166.1760547 | 165.95 |
| 979.4733367 | 182.1563636 | 181.93 |
| 979.3904099 | 198.0412672 | 197.81 |
| 979.3079752 | 213.8318978 | 213.6  |
| 979.2260268 | 229.5293677 | 229.3  |
| 979.1445591 | 245.1347699 | 244.9  |
| 979.0635664 | 260.649178  | 260.42 |
| 978.9830432 | 276.0736469 | 275.84 |
| 978.9029842 | 291.4092135 | 291.18 |
| 978.8233839 | 306.6568968 | 306.43 |
| 978.7442372 | 321.8176982 | 321.59 |
| 978.665539  | 336.8926022 | 336.66 |
| 978.5872841 | 351.8825767 | 351.65 |
| 978.5094676 | 366.7885734 | 366.56 |
| 978.4320846 | 381.6115278 | 381.38 |
| 978.3551304 | 396.3523602 | 396.12 |
| 978.2786001 | 411.0119755 | 410.78 |
| 978.2024892 | 425.5912637 | 425.36 |
| 978.1267931 | 440.0911004 | 439.86 |
| 978.0515072 | 454.5123468 | 454.28 |
| 977.9766272 | 468.858502  | 468.62 |
| 977.9021487 | 483.124444  | 482.89 |
| 977.8280674 | 497.3129497 | 497.08 |
| 977.7543791 | 511.4281735 | 511.2  |
| 977.6810797 | 525.4689103 | 525.24 |
| 977.6081651 | 539.4359421 | 539.21 |
| 977.5356312 | 553.3300386 | 553.1  |
| 977.4634741 | 567.1519577 | 566.92 |
| 977.39169   | 580.9024454 | 580.67 |
| 977.3202748 | 594.5822362 | 594.35 |
| 977.249225  | 608.1920533 | 607.96 |
| 977.1785368 | 621.732089  | 621.5  |
| 977.1082065 | 635.2046045 | 634.97 |
| 977.0382305 | 648.6087308 | 648.38 |
| 976.9686053 | 661.9456682 | 661.71 |
| 976.8993273 | 675.2165087 | 674.99 |
| 976.8303931 | 688.4206473 | 688.19 |
| 976.7617994 | 701.5599996 | 701.33 |
| 976.6935427 | 714.6347849 | 714.4  |
| 976.6256198 | 727.6456345 | 727.41 |
| 976.5580274 | 740.5831707 | 740.36 |
| 976.4907623 | 753.4780067 | 753.25 |
| 976.4238214 | 766.3007469 | 766.07 |
| 976.3572016 | 779.061987  | 778.83 |
| 976.2908998 | 791.7623139 | 791.53 |
| 976.2249129 | 804.4023065 | 804.17 |
| 976.1592381 | 816.9825354 | 816.75 |
| 976.0938723 | 829.5035629 | 829.27 |
| 976.0288126 | 841.9659437 | 841.74 |
| 975.9640563 | 854.3702247 | 854.14 |
| 975.8996005 | 866.7169449 | 866.49 |
| 975.8354424 | 879.0066363 | 878.78 |
| 975.7715792 | 891.2398231 | 891.01 |
| 975.7080084 | 903.4170226 | 903.19 |

## Permeability Data

## FLOW DATA

## Variables

|                                 |               |
|---------------------------------|---------------|
| Area (in <sup>2</sup> )         | 1             |
| Dynamic Viscosity N2 (lbm/in*s) | 0.00000093492 |
| Ceramic Flow Length (in)        | 0.25          |
| Insulation Flow Length (in)     | 0.5           |
| Cloth Flow Length (in)          | 0.03125       |

Material: Silicon Carbide Foam  
100 PPI, 10 - 15% density

## Delta\_h (in) Trials

| Mdot (L/min) | Q (in <sup>3</sup> /s) | #1 (50 psi) | #2 (50 psi) | #3 (100 psi) | #4 (100 psi) | Average | PSI         | K (in <sup>2</sup> ) |
|--------------|------------------------|-------------|-------------|--------------|--------------|---------|-------------|----------------------|
| 10           | 0.01413                | 0.0313      | 0.1250      | 0.0625       | 0.0625       | 0.0703  | 0.002539688 | 3.36813E-09          |
| 20           | 0.02826                | 0.0625      | 0.1250      | 0.0938       | 0.1250       | 0.1016  | 0.003668438 | 4.66356E-09          |
| 30           | 0.04239                | 0.1563      | 0.1563      | 0.1250       | 0.1875       | 0.1563  | 0.00564375  | 4.54697E-09          |
| 40           | 0.05652                | 0.1875      | 0.250       | 0.1875       | 0.281        | 0.227   | 0.008183438 | 4.18112E-09          |
| 50           | 0.07065                | 0.250       | 0.313       | 0.250        | 0.313        | 0.281   | 0.01015875  | 4.21016E-09          |

Material: Reticulated Vitreous Carbon Foam  
100 PPI, 21 - 24% density, RVC compressed 7 - 8 times from 3% density

## Delta\_h (in) Trials

| Mdot (L/min) | Q (in <sup>3</sup> /s) | #1 (50 psi) | #2 (50 psi) | #3 (100 psi) | #4 (100 psi) | Average | PSI         | K (in <sup>2</sup> ) |
|--------------|------------------------|-------------|-------------|--------------|--------------|---------|-------------|----------------------|
| 10           | 0.01413                | 0.438       | 0.563       | 0.500        | 0.500        | 0.500   | 0.01806     | 4.73643E-10          |
| 20           | 0.02826                | 0.969       | 1.000       | 1.063        | 1.063        | 1.023   | 0.036966563 | 4.62796E-10          |
| 30           | 0.04239                | 1.563       | 1.625       | 1.750        | 1.813        | 1.688   | 0.0609525   | 4.21016E-10          |
| 40           | 0.05652                | 2.41        | 2.38        | 2.44         | 2.50         | 2.43    | 0.087760313 | 3.8988E-10           |
| 50           | 0.07065                | 3.28        | 3.31        | 3.31         | 3.38         | 3.32    | 0.119929688 | 3.56625E-10          |

Material: PS 6448 Durablanket - S 6# - 1/2"

## Delta\_h (in) Trials

| Mdot (L/min) | Q (in <sup>3</sup> /s) | #1 (50 psi) | #2 (50 psi) | #3 (100 psi) | #4 (100 psi) | Average | PSI         | K (in <sup>2</sup> ) |
|--------------|------------------------|-------------|-------------|--------------|--------------|---------|-------------|----------------------|
| 10           | 0.01413                | 1.125       | 1.250       | 1.188        | 1.281        | 1.211   | 0.043739063 | 3.91137E-10          |
| 20           | 0.02826                | 2.38        | 2.50        | 2.44         | 2.56         | 2.47    | 0.08917125  | 3.83711E-10          |
| 30           | 0.04239                | 3.88        | 3.88        | 3.81         | 3.88         | 3.86    | 0.139400625 | 3.68176E-10          |
| 40           | 0.05652                | 5.19        | 5.06        | 5.31         | 5.31         | 5.22    | 0.18850125  | 3.63032E-10          |
| 50           | 0.07065                | 6.63        | 6.44        | 6.75         | 6.75         | 6.64    | 0.239859375 | 3.56625E-10          |

Material: Refrasil UC100-96 Standard Woven Fabric  
NOTE: Only one trial performed to check feasibility of wrapping  
over insulation for protective purposes.

| Mdot (L/min) | Q (in <sup>3</sup> /s) | #1 (100 psi) | PSI       | K (in <sup>2</sup> ) |
|--------------|------------------------|--------------|-----------|----------------------|
| 10           | 0.01413                | 2.13         | 0.076755  | 1.39307E-11          |
| 20           | 0.02826                | 5.44         | 0.1964025 | 1.08883E-11          |
| 30           | 0.04239                | 12.50        | 0.4515    | 7.10464E-12          |
| 40           | 0.05652                | 19.75        | 0.71337   | 5.99548E-12          |
| 50           | 0.07065                | 27.5         | 0.9933    | 5.38231E-12          |

```

function heat_trans_miller

%This program solves the heat equation in 2D cylindrical for r and z. There
%is an internal tube of constant temperature T1 enclosed by a larger tube
%that extends on all sides of the internal tube. The larger tube has a
%convective boundary condition. ALL UNITS ARE SI (K, m, W, s)

close all
clear all

%-----inputs-----
T_inner      = 1300; %temperature at inner tube surface (K)
T_amb       = 300; %Ambient air temperature (K)
T_error_allowed = eps; %allowed temperature difference at max point (K)

k           = 0.4; %thermal conductivity of insulation (area between
tubes) (W/m K)
h           = 10; %convective heat trans. coef. for external BC
(W/m^2 K)

r_inner     = 0.03; %radius of internal tube (m)
r_outer     = 0.2; %radius of external tube (m)

z1          = 0.1; %z coordinate of ext. tube start (m)
z2          = 0.6; %z coordinate of int. tube start (m)
z3          = 0.7; %z coordinate of ext. tube end (m)

dr_in       = 10; %number of radial divisions for inner radius
dr_out      = 10; %number of radial divisions for area between tubes

dz1         = 10; %number of length divisions for 0 < z < z1
dz2         = 50; %number of length divisions for z1 < z < z2
dz3         = 10; %number of length divisions for z2 < z < z3

%-----grid-----
%radial grid
delr_in     = r_inner/dr_in; %0 =< r =< r_inner
r_in        = 0:delr_in:r_inner;

delr_out    = (r_outer-r_inner)/dr_out; %r_inner < r =< r_outer
r_out       = (r_inner+delr_out):delr_out:r_outer;

R           = [r_in r_out]; %radial grid

R_size      = dr_in+dr_out+1; %elements in radial grid

%axial grid
delz1       = z1/dz1; % 0 =< z =< z1
z_1         = 0:delz1:z1;

delz2       = (z2-z1)/dz2; %z1 < z =< z2
z_2         = (z1+delz2):delz2:z2;

```

```

delz3      = (z3-z2)/dz3;           %z2 < z =< z3
z_3        = (z2+delz3):delz3:z3;

Z          = [z_1 z_2 z_3];        %axial grid
Z_size     = dz1+dz2+dz3+1;       %elements in axial grid

%-----Initialize temperature-----
for i=1:R_size
    for j=1:Z_size
        T(i,j)=T_amb;
    end
end

%-----Set temperature at inner tube-----
for i=1:(dr_in+1)
    for j=(dz1+1):(dz2+dz1+1)
        T(i,j)=T_inner;
    end
end

%-----Interior node coefficients-----
for i=2:(R_size-1)
    rn(i)=R(i)+((R(i+1)-R(i))/2);
    drn(i)=R(i+1)-R(i);

    rs(i)=R(i)-((R(i)-R(i-1))/2);
    drs(i)=R(i)-R(i-1);
end
for j=2:(Z_size-1)
    ze(j)=Z(j)+((Z(j+1)-Z(j))/2);
    dze(j)=Z(j+1)-Z(j);

    zw(j)=Z(j)-((Z(j)-Z(j-1))/2);
    dzw(j)=Z(j)-Z(j-1);
end
for i=2:(R_size-1)
    for j=2:(Z_size-1)
        An(i,j)=(k*rn(i)/drn(i))*(ze(j)-zw(j));
        As(i,j)=(k*rs(i)/drs(i))*(ze(j)-zw(j));
        Ae(i,j)=(k/(2*dze(j)))*((rn(i)^2)-(rs(i)^2));
        Aw(i,j)=(k/(2*dzw(j)))*((rn(i)^2)-(rs(i)^2));
        Ap(i,j)=An(i,j)+As(i,j)+Ae(i,j)+Aw(i,j);
    end
end

%-----Boundary node coefficients-----
%R=0, Z=0 and Z=Z3
rn(1)=R(1)+((R(2)-R(1))/2);
drn(1)=R(2)-R(1);

ze(1)=Z(1)+((Z(2)-Z(1))/2);
dze(1)=Z(2)-Z(1);

ze(Z_size)=z3;

```

```

zw(Z_size)=Z(Z_size)-((Z(Z_size)-Z(Z_size-1))/2);
dzw(Z_size)=Z(Z_size)-Z(Z_size-1);

An(1,1)=(k*rn(1)/drn(1))*ze(1);
As(1,1)=0;
Ae(1,1)=(k/(2*dze(1)))*rn(1)^2;
Aw(1,1)=(h/2)*rn(1)^2;
Ap(1,1)=An(1,1)+As(1,1)+Ae(1,1)+Aw(1,1);

An(1,Z_size)=(k*rn(1)/drn(1))*(Z(Z_size)-zw(Z_size));
As(1,Z_size)=0;
Ae(1,Z_size)=(h/2)*rn(1)^2;
Aw(1,Z_size)=(k/(2*dzw(Z_size)))*rn(1)^2;
Ap(1,Z_size)=An(1,Z_size)+As(1,Z_size)+Ae(1,Z_size)+Aw(1,Z_size);

%R=0, 0<Z<Z1 and Z2<Z<Z3
for j=2:dz1
    An(1,j)=(k*rn(1)/drn(1))*(ze(j)-zw(j));
    As(1,j)=0;
    Ae(1,j)=(k/(2*dze(j)))*rn(1)^2;
    Aw(1,j)=(k/(2*dzw(j)))*rn(1)^2;
    Ap(1,j)=An(1,j)+As(1,j)+Ae(1,j)+Aw(1,j);
end
for j=(dz2+1):(Z_size-1)
    An(1,j)=(k*rn(1)/drn(1))*(ze(j)-zw(j));
    As(1,j)=0;
    Ae(1,j)=(k/(2*dze(j)))*rn(1)^2;
    Aw(1,j)=(k/(2*dzw(j)))*rn(1)^2;
    Ap(1,j)=An(1,j)+As(1,j)+Ae(1,j)+Aw(1,j);
end

%R=R2, 0<Z<Z3
rn(R_size)=r_outer; %this is only to keep rn and rs the same dimensions
rs(R_size)=R(R_size)-((R(R_size)-R(R_size-1))/2);
drs(R_size)=R(R_size)-R(R_size-1);
for j=2:(Z_size-1)
    An(R_size,j)=h*R(R_size)*(ze(j)-zw(j));
    As(R_size,j)=(k*rs(R_size)/drs(R_size))*(ze(j)-zw(j));
    Ae(R_size,j)=(k/(2*dze(j)))*((R(R_size)^2)-(rs(R_size)^2));
    Aw(R_size,j)=(k/(2*dzw(j)))*((R(R_size)^2)-(rs(R_size)^2));
    Ap(R_size,j)=An(R_size,j)+As(R_size,j)+Ae(R_size,j)+Aw(R_size,j);
end

%R=R2, Z=0 and Z=Z3
An(R_size,1)=h*R(R_size)*ze(1);
As(R_size,1)=(k*rs(R_size)/drs(R_size))*ze(1);
Ae(R_size,1)=(k/(2*dze(1)))*(R(R_size)^2-rs(R_size)^2);
Aw(R_size,1)=(h/2)*(R(R_size)^2-rs(R_size)^2);
Ap(R_size,1)=An(R_size,1)+As(R_size,1)+Ae(R_size,1)+Aw(R_size,1);

An(R_size,Z_size)=h*R(R_size)*(Z(Z_size)-zw(Z_size));
As(R_size,Z_size)=(k*rs(R_size)/drs(R_size))*(Z(Z_size)-zw(Z_size));
Ae(R_size,Z_size)=(h/2)*(R(R_size)^2-rs(R_size)^2);
Aw(R_size,Z_size)=(k/(2*dzw(Z_size)))*(R(R_size)^2-rs(R_size)^2);

```

```
Ap(R_size,Z_size)=An(R_size,Z_size)+As(R_size,Z_size)+Ae(R_size,Z_size)+Aw(R_size,Z_size);
```

```
%0<R<R2, Z=0 and Z=Z3
```

```
for i=2:(R_size-1)
    An(i,1)=(k*rn(i)/drn(i))*ze(1);
    As(i,1)=(k*rs(i)/drs(i))*ze(1);
    Ae(i,1)=(k/(2*dze(1)))*((rn(i)^2)-(rs(i)^2));
    Aw(i,1)=(h/2)*((rn(i)^2)-(rs(i)^2));
    Ap(i,1)=An(i,1)+As(i,1)+Ae(i,1)+Aw(i,1);

    An(i,Z_size)=(k*rn(i)/drn(i))*(Z(Z_size)-zw(Z_size));
    As(i,Z_size)=(k*rs(i)/drs(i))*(Z(Z_size)-zw(Z_size));
    Ae(i,Z_size)=(h/2)*((rn(i)^2)-(rs(i)^2));
    Aw(i,Z_size)=(k/(2*dzw(Z_size)))*((rn(i)^2)-(rs(i)^2));
    Ap(i,Z_size)=An(i,Z_size)+As(i,Z_size)+Ae(i,Z_size)+Aw(i,Z_size);
end
```

```
%-----Specify error terms-----
```

```
T_error=T_error_allowed+1;
k=1;
for i=1:R_size
    for j=1:Z_size
        T_old(i,j)=T_inner;
    end
end
```

```
%-----Solve set of equations-----
```

```
while T_error>=T_error_allowed
    k=k+1;
    for i=1:R_size
        for j=1:Z_size
            if i==1
                if j==1
                    T(i,j)=(An(i,j)*T(i+1,j)+Ae(i,j)*T(i,j+1)+Aw(i,j)*T_amb)/Ap(i,j);
                elseif j>1 && j<(dz1+1)
                    T(i,j)=(An(i,j)*T(i+1,j)+Ae(i,j)*T(i,j+1)+Aw(i,j)*T(i,j-1))/Ap(i,j);
                elseif j>(dz2+dz1+1) && j<(Z_size)
                    T(i,j)=(An(i,j)*T(i+1,j)+Ae(i,j)*T(i,j+1)+Aw(i,j)*T(i,j-1))/Ap(i,j);
                elseif j==Z_size
                    T(i,j)=(An(i,j)*T(i+1,j)+Ae(i,j)*T_amb+Aw(i,j)*T(i,j-1))/Ap(i,j);
                end
            end
            if i>1 && i<R_size
                if j==1
                    T(i,j)=(An(i,j)*T(i+1,j)+As(i,j)*T(i-1,j)+Ae(i,j)*T(i,j+1)+Aw(i,j)*T_amb)/Ap(i,j);
                elseif j==Z_size
                    T(i,j)=(An(i,j)*T(i+1,j)+As(i,j)*T(i-1,j)+Ae(i,j)*T_amb+Aw(i,j)*T(i,j-1))/Ap(i,j);
                end
            end
        end
    end
end
```

```

        if i==R_size
            if j==1
                T(i,j)=(An(i,j)*T_amb+As(i,j)*T(i-
1,j)+Ae(i,j)*T(i,j+1)+Aw(i,j)*T_amb)/Ap(i,j);
            elseif j>1 && j<Z_size
                T(i,j)=(An(i,j)*T_amb+As(i,j)*T(i-
1,j)+Ae(i,j)*T(i,j+1)+Aw(i,j)*T(i,j-1))/Ap(i,j);
            elseif j==Z_size
                T(i,j)=(An(i,j)*T_amb+As(i,j)*T(i-
1,j)+Ae(i,j)*T_amb+Aw(i,j)*T(i,j-1))/Ap(i,j);
            end
        end
        if i>1 && i<R_size
            if j>1 && j<(dz1+1)
                T(i,j)=(An(i,j)*T(i+1,j)+As(i,j)*T(i-
1,j)+Ae(i,j)*T(i,j+1)+Aw(i,j)*T(i,j-1))/Ap(i,j);
            elseif j>(dz2+dz1+1) && j<Z_size
                T(i,j)=(An(i,j)*T(i+1,j)+As(i,j)*T(i-
1,j)+Ae(i,j)*T(i,j+1)+Aw(i,j)*T(i,j-1))/Ap(i,j);
            end
        end
        if i>(dr_in+1) && i<R_size
            if j>=(dz1+1) && j<=(dz2+dz1+1)
                T(i,j)=(An(i,j)*T(i+1,j)+As(i,j)*T(i-
1,j)+Ae(i,j)*T(i,j+1)+Aw(i,j)*T(i,j-1))/Ap(i,j);
            end
        end
    end
end
end
for i=1:R_size
    for j=1:Z_size
        T_er(i,j)=abs(T(i,j)-T_old(i,j));
    end
end
T_old=T;
T_er_row_max=max(T_er);
T_error=max(T_er_row_max);
end

```

```

%-----Plotting-----
surf(Z,R,T)
colorbar
view(2)
axis equal
title('Temperature Profile for Insulated Coil')
xlabel('Z (m)')
ylabel('R (m)')

```

```

%-----Energy balance at each CV-----
for i=1:R_size
    for j=1:Z_size
        An(i,j)=2*pi*An(i,j);
        As(i,j)=2*pi*As(i,j);
        Ae(i,j)=2*pi*Ae(i,j);
        Aw(i,j)=2*pi*Aw(i,j);
    end
end

```

```

        Ap(i,j)=An(i,j)+As(i,j)+Ae(i,j)+Aw(i,j);
    end
end

%-----Solve heat flux equations-----
for i=1:R_size
    for j=1:Z_size
        if i==1
            if j==1
                q(i,j)=(An(i,j)*T(i+1,j)+Ae(i,j)*T(i,j+1)+Aw(i,j)*T_amb)-
Ap(i,j)*T(i,j);
            elseif j>1 && j<(dz1+1)
                q(i,j)=(An(i,j)*T(i+1,j)+Ae(i,j)*T(i,j+1)+Aw(i,j)*T(i,j-1))-
Ap(i,j)*T(i,j);
            elseif j>(dz2+dz1+1) && j<(Z_size)
                q(i,j)=(An(i,j)*T(i+1,j)+Ae(i,j)*T(i,j+1)+Aw(i,j)*T(i,j-1))-
Ap(i,j)*T(i,j);
            elseif j==Z_size
                q(i,j)=(An(i,j)*T(i+1,j)+Ae(i,j)*T_amb+Aw(i,j)*T(i,j-1))-
Ap(i,j)*T(i,j);
            end
        end
        if i>1 && i<R_size
            if j==1
                q(i,j)=(An(i,j)*T(i+1,j)+As(i,j)*T(i-
1,j)+Ae(i,j)*T(i,j+1)+Aw(i,j)*T_amb)-Ap(i,j)*T(i,j);
            elseif j==Z_size
                q(i,j)=(An(i,j)*T(i+1,j)+As(i,j)*T(i-
1,j)+Ae(i,j)*T_amb+Aw(i,j)*T(i,j-1))-Ap(i,j)*T(i,j);
            end
        end
        if i==R_size
            if j==1
                q(i,j)=(An(i,j)*T_amb+As(i,j)*T(i-
1,j)+Ae(i,j)*T(i,j+1)+Aw(i,j)*T_amb)-Ap(i,j)*T(i,j);
            elseif j>1 && j<Z_size
                q(i,j)=(An(i,j)*T_amb+As(i,j)*T(i-
1,j)+Ae(i,j)*T(i,j+1)+Aw(i,j)*T(i,j-1))-Ap(i,j)*T(i,j);
            elseif j==Z_size
                q(i,j)=(An(i,j)*T_amb+As(i,j)*T(i-
1,j)+Ae(i,j)*T_amb+Aw(i,j)*T(i,j-1))-Ap(i,j)*T(i,j);
            end
        end
        if i>1 && i<R_size
            if j>1 && j<(dz1+1)
                q(i,j)=(An(i,j)*T(i+1,j)+As(i,j)*T(i-
1,j)+Ae(i,j)*T(i,j+1)+Aw(i,j)*T(i,j-1))-Ap(i,j)*T(i,j);
            elseif j>(dz2+dz1+1) && j<Z_size
                q(i,j)=(An(i,j)*T(i+1,j)+As(i,j)*T(i-
1,j)+Ae(i,j)*T(i,j+1)+Aw(i,j)*T(i,j-1))-Ap(i,j)*T(i,j);
            end
        end
        if i>(dr_in+1) && i<R_size
            if j>=(dz1+1) && j<=(dz2+dz1+1)
                q(i,j)=(An(i,j)*T(i+1,j)+As(i,j)*T(i-
1,j)+Ae(i,j)*T(i,j+1)+Aw(i,j)*T(i,j-1))-Ap(i,j)*T(i,j);
            end
        end
    end
end

```

```

        end
    end
end
for i=1:R_size
    for j=1:Z_size
        q(i,j)=abs(q(i,j));
    end
end
q_max_row=max(q);
Energy_storage_at_CV_with_highest_energy=max(q_max_row)

%-----Surface heat flux-----
q_out=0;
for i=1:R_size
    A_s_side(i)=pi*(rn(i)^2-rs(i)^2);
    q_out_1=h*A_s_side(i)*(T(i,1)-T_amb);
    q_out_3=h*A_s_side(i)*(T(i,Z_size)-T_amb);
    q_out=q_out+q_out_1+q_out_3;
end
for j=1:Z_size
    A_s_top(j)=2*pi*r_outer*(ze(j)-zw(j));
    q_out_2=h*A_s_top(j)*(T(R_size,j)-T_amb);
    q_out=q_out+q_out_2;
end
total_heat_flux_in_watts=q_out

```

Table 2. Nozzle Data

| <u>D(in)</u> | <u>D(m)</u> | <u>A<sub>ct</sub></u> | <u>U<sub>mt</sub></u> | <u>Red</u> | <u>Δp(psi)</u> |
|--------------|-------------|-----------------------|-----------------------|------------|----------------|
| 0.01         | 0.000254    | 5.06707E-08           | 6096                  | 9002.233   | 2272158        |
| 0.02         | 0.000508    | 2.02683E-07           | 1524                  | 4501.116   | 87390.01       |
| 0.03         | 0.000762    | 4.56037E-07           | 677.3333333           | 3000.744   | 13135.51       |
| 0.04         | 0.001016    | 8.10732E-07           | 381                   | 2250.558   | 3443.043       |
| 0.05         | 0.00127     | 1.26677E-06           | 243.84                | 1800.447   | 1223.03        |
| 0.06         | 0.001524    | 1.82415E-06           | 169.3333333           | 1500.372   | 526.3233       |
| 0.07         | 0.001778    | 2.48287E-06           | 124.4081633           | 1286.033   | 258.5037       |
| 0.08         | 0.002032    | 3.24293E-06           | 95.25                 | 1125.279   | 139.839        |
| 0.09         | 0.002286    | 4.10433E-06           | 75.25925926           | 1000.248   | 81.42992       |
| 0.1          | 0.00254     | 5.06707E-06           | 60.96                 | 900.2233   | 50.25106       |
| 0.11         | 0.002794    | 6.13116E-06           | 50.38016529           | 818.3848   | 32.49939       |
| 0.12         | 0.003048    | 7.29659E-06           | 42.33333333           | 750.186    | 21.84772       |
| 0.13         | 0.003302    | 8.56336E-06           | 36.07100592           | 692.4794   | 15.17158       |
| 0.14         | 0.003556    | 9.93147E-06           | 31.10204082           | 643.0166   | 10.83047       |
| 0.15         | 0.00381     | 1.14009E-05           | 27.09333333           | 600.1488   | 7.917524       |
| 0.16         | 0.004064    | 1.29717E-05           | 23.8125               | 562.6395   | 5.90903        |
| 0.17         | 0.004318    | 1.46438E-05           | 21.09342561           | 529.5431   | 4.490876       |
| 0.18         | 0.004572    | 1.64173E-05           | 18.81481481           | 500.124    | 3.468377       |
| 0.19         | 0.004826    | 1.82921E-05           | 16.88642659           | 473.8017   | 2.717328       |
| 0.2          | 0.00508     | 2.02683E-05           | 15.24                 | 450.1116   | 2.156433       |
| 0.21         | 0.005334    | 2.23458E-05           | 13.82312925           | 428.6777   | 1.731251       |
| 0.22         | 0.005588    | 2.45246E-05           | 12.59504132           | 409.1924   | 1.404569       |
| 0.23         | 0.005842    | 2.68048E-05           | 11.52362949           | 391.4014   | 1.150475       |
| 0.24         | 0.006096    | 2.91864E-05           | 10.58333333           | 375.093    | 0.950618       |
| 0.25         | 0.00635     | 3.16692E-05           | 9.7536                | 360.0893   | 0.791805       |
| 0.26         | 0.006604    | 3.42534E-05           | 9.017751479           | 346.2397   | 0.664413       |
| 0.27         | 0.006858    | 3.6939E-05            | 8.362139918           | 333.416    | 0.561336       |
| 0.28         | 0.007112    | 3.97259E-05           | 7.775510204           | 321.5083   | 0.477258       |
| 0.29         | 0.007366    | 4.26141E-05           | 7.248513674           | 310.4218   | 0.408167       |
| 0.3          | 0.00762     | 4.56037E-05           | 6.773333333           | 300.0744   | 0.350994       |
| 0.31         | 0.007874    | 4.86946E-05           | 6.3433923             | 290.3946   | 0.303378       |
| 0.32         | 0.008128    | 5.18868E-05           | 5.953125              | 281.3198   | 0.263479       |
| 0.33         | 0.008382    | 5.51804E-05           | 5.597796143           | 272.7949   | 0.229858       |
| 0.34         | 0.008636    | 5.85754E-05           | 5.273356401           | 264.7715   | 0.201375       |
| 0.35         | 0.00889     | 6.20717E-05           | 4.976326531           | 257.2066   | 0.177124       |
| 0.36         | 0.009144    | 6.56693E-05           | 4.703703704           | 250.062    | 0.156379       |
| 0.37         | 0.009398    | 6.93683E-05           | 4.452885318           | 243.3036   | 0.138553       |
| 0.38         | 0.009652    | 7.31686E-05           | 4.221606648           | 236.9009   | 0.123171       |
| 0.39         | 0.009906    | 7.70702E-05           | 4.007889546           | 230.8265   | 0.109845       |

|     |         |             |      |          |          |
|-----|---------|-------------|------|----------|----------|
| 0.4 | 0.01016 | 8.10732E-05 | 3.81 | 225.0558 | 0.098257 |
|-----|---------|-------------|------|----------|----------|